European volcanological supersite in Iceland: a monitoring system and network for the future

Report

D4.3 – A manuscript discussing compositional time series of historical Grímsvötn tephra

Work Package:	*Evaluation of known Eruption Source Parameters*
Work Package number:	*4*
Deliverable:	*A manuscript discussing compositional time series of historical Grímsvötn tephra*
Deliverable number:	*4.3*
Type of Activity:	*RTD*
Responsible activity leader:	*Ilyinskaya Evgenia*
Responsible participant:	*LMV, Université Blaise Pascal, Clermont-Ferrand*
Authors:	*Olgeir Sigmarsson (LMV), Marion Carpentier (LMV), Gudrun Larsen (UI) and Magnus Gudmundsson (UI)*

Type of Deliverable:	*Report*	*[X]*	*Demonstrator*	*[ ]*
	Prototype	*[ ]*	*Other*	*[ ]*
Dissemination level:	*Public*	*[X]*	*Restricted Designated Group*	*[ ]*
	Prog. Participants (FP7)	*[ ]*	*Confidential (consortium)*	*[ ]*

Seventh Framework Programme
EC project number: 308377

Elsevier Editorial System(tm) for Earth and Planetary Science Letters
Manuscript Draft

Manuscript Number:

Title: New constraints on Grímsvötn magmatic system inferred from ice-kept historical tephra

Article Type: Letters

Keywords: Grímsvötn volcano, tephra, magma volumes, plumbing system, magma fluxes, magma differentiation rates

Corresponding Author: Dr. Olgeir Sigmarsson,

Corresponding Author's Institution:

First Author: Olgeir Sigmarsson

Order of Authors: Olgeir Sigmarsson; Olgeir Sigmarsson; Marion Carpentier; Gudrun Larsen

Abstract: Compositional time-series can unravel the dynamics of magma systems beneath active volcanoes. In ideal cases, parameters such as magma flux, reservoir geometry, its lifetime and the transfer time of magma can be inferred from the compositional variations. Quantification of these parameters will improve the understanding of volcano behaviour and, thus, the predictions of their future activity. From the Grímsvötn volcano, Iceland, ice-kept historical tephra has been precisely analysed for trace element concentrations and Sr-, Nd- and Pb isotope ratios. Most of the tephra have uniform isotope ratios suggesting cogenetic magma evolution. Temporal variations of the tephra compositions over the last eight centuries reveal linear decrease and increase in compatible and incompatible trace element concentrations, respectively, caused by eruptions of increasingly differentiated basaltic magma with time. The trace element systematic is readily explained by polybaric fractional crystallization suggesting evolution in more than one magma reservoir beneath Grímsvötn volcano.

The simple magma differentiation and the temporal variations allow estimation of diminishing melt fraction in the magma system as a function of time. It decreased by 35% over the last 800 years yielding slow magma differentiation rate, or ~4 x10-4 yr-1. Magma production rate for the 20th century suggests that approximately 8 km3 of basalts have erupted over the last 8 centuries, whereas the magma reservoir have decreased from approximately 100 km3 to 50-90 km3. Without magma recharging and similar behaviour as during the last eight centuries, evolved basalts will be produced at Grímsvötn for the next 500-1000 yrs.

Suggested Reviewers: Aaron Pietruszka
apietruszka@usgs.gov
Has studied isotope and trace element variations as a fonction of time on Kilauea

Michael Garcia
garcia@soest.hawaii.edu
Has studied isotope and trace element variations as a fonction of time on Kilauea

Tore Prestik
tore.prestvik@ntnu.no
Has studied the volcanism in the region. Expert on Öræfajökull.

Ken Sims
ksims7@uwyo.edu
Geochemist interested in volcanic/magmatic processes

Stephen Blake
stephen.blake@open.ac.uk
Expert in physical volcanology

Opposed Reviewers:

Cover Letter

Reykjavík, 7 March 2015

Dear Editor,

We would like to submit a manuscript describing temporal variations in the composition of Grímsvötn tephra. The regular variability is deciphered from high-precision trace and isotope analyses of the bulk tephra that were sampled from the Vatnajökull glacier. This unique time series allows to discuss magma fluxes and reservoir changes over time that lead to better understanding of the volcanoe's behaviour and potential future activity.

Yours sincerely,

Olgeir Sigmarsson

New constraints on Grímsvötn magmatic system inferred from ice-kept historical tephra

Olgeir Sigmarsson[1,2], Marion Carpentier[1], Gudrun Larsen[2] and Magnus T. Gudmundsson[2]

1- Laboratoire Magmas et Volcans, CNRS-Université Blaise Pascal, 63038 Clermont-Ferrand, France
2- Institute of Earth Sciences, University of Iceland, 101 Reykjavik, Iceland

Corresponding author: Olgeir Sigmarsson (olgeir@hi.is)

Abstract

Compositional time-series can unravel the dynamics of magma systems beneath active volcanoes. In ideal cases, parameters such as magma flux, reservoir geometry, its lifetime and the transfer time of magma can be inferred from the compositional variations. Quantification of these parameters will improve the understanding of volcano behaviour and, thus, the predictions of their future activity. From the Grímsvötn volcano, Iceland, ice-kept historical tephra has been precisely analysed for trace element concentrations and Sr-, Nd- and Pb isotope ratios. Most of the tephra have uniform isotope ratios suggesting cogenetic magma evolution. Temporal variations of the tephra compositions over the last eight centuries reveal linear decrease and increase in compatible and incompatible trace element concentrations, respectively, caused by eruptions of increasingly differentiated basaltic magma with time. The trace element systematic is readily explained by polybaric fractional crystallization suggesting evolution in more than one magma reservoir beneath Grímsvötn volcano.

The simple magma differentiation and the temporal variations allow estimation of diminishing melt fraction in the magma system as a function of time. It decreased by 35% over the last 800 years yielding slow magma differentiation rate, or ~4 x10^{-4} yr^{-1}. Magma production rate for the 20th century suggests that approximately 8 km^3 of basalts have erupted over the last 8 centuries, whereas the magma reservoir have decreased from approximately 100 km^3 to 50-90 km^3. Without magma recharging and similar behaviour as during the last eight centuries, evolved basalts will be produced at Grímsvötn for the next 500-1000 yrs.

Keywords: Grímsvötn volcano, tephra, magma volumes, plumbing system, magma fluxes, magma differentiation rates

1 Introduction

Future magmatic activity of an active volcano is probably best estimated from its past activity. Detailed time series of magma composition erupted should, in principle, allow predictions of likely future magma compositions to be erupted. Such time series can also constrain the size of magma systems, their configuration and allow magma residence time to be estimated (e.g. Pietruszka and Garcia, 1999; Albarède, 1993; Sigmarsson et al., 2006).

The most active volcano of Iceland, the subglacial Grímsvötn volcano, has erupted approximately every decade on average during the historical time. The phreatomagmatic nature of its eruptions has generated extensive tephra record that allows construction of detailed compositional time series. Here are presented high-precision trace element concentrations and the isotope ratios of Sr, Nd and Pb in bulk tephra from a sample suite that corresponds to the last eight centuries of volcanic activity. The results permit constraining the magma differentiation mechanism, discussion of magma differentiation rates, magma fluxes and reservoir volume beneath Grímsvötn as well as speculations of possible future activity.

2 Geological setting

Grímsvötn volcano is the most active volcano of Iceland, due to its location above the Iceland mantle plume centre. Together with the Laki eruption fissure, the Grímsvötn central volcano forms a volcanic system, which together with other active volcanic systems composes the Neovolcanic zones of Iceland (Fig. 1). A shallow magma chamber (depth: 2-3 km) has been seismically identified (Alfaro et al., 2007) and inferred from deformation studies (Hreinsdottir et al., 2014). A deeper magma reservoir with an oblate or a sill-like form is suggested by longer deformation time series and slow seismic velocity of regional earthquakes illuminating the Grímsvötn interior (Reverso et al., 2014; Alfaro et al., 2007). A hypothetical, even deeper, third magma reservoir, which may or may not be located at the crust-mantle interface, cannot be currently detected with the GPS network due to the present poor spatial resolution caused by the glacial cover according to Reverso et al. (2014).

The intense volcanic activity at Grímsvötn and resulting geothermal system has formed a caldera lake beneath the Vatnajökull ice-cap (e.g. Björnsson et al., 1982; Björnsson and Gudmundsson, 1993). This lake is periodically emptied in subglacial water bursts (jökulhlaup) that occasionally may cause sufficient pressure relief to initiate an eruption (e.g. Thorarinsson, 1974). The water-magma interaction results in formation of basaltic tephra due to rapid quench upon eruption, although such interaction is minimized in the largest eruptions when high magma flux may hold water from entering the crater (Hreinsdottir et al., 2014; Sigmarsson et al 2013). The tephra produced falls on and outside the glacier depending on the wind direction and strength as well as the eruption magnitude. Proximal tephra is buried during the winter snowfall in the accumulation area of the glacier and are transported with the glacier movements

down to the ablation area and the outlet glaciers. Distal tephra falling outside the glacier is deposited on soil and can be peserved for thousand of years before complete palagonitization (Oladottir et al., 2005).

The basaltic tephra from Grímsvötn is principally composed of glass with 1-5% plagioclase, olivine and clinopyroxene crystals in decreasing abundance. Titatnomagnetites and Fe-rich sulphides are rare and have only been identified in the 2011 eruption yet (Sigmarsson et al., 2013). The basalt composition has remained fairly uniform through the Holocene, namely evolved quartz normative tholeiite (Oladottir et al., 2011). Subtle variations are observed in the prehistoric tephra glass with a possible contemporaneous eruption of two types of qz-tholeiites. Historical tephra have restricted major element composition and variability within each eruption is limited (e.g. Sigmarsson et al., 2000). Concentrations of highly incompatible trace elements (U and Th) in the 15 km^3 of the Laki eruption varied only by 7%, explained by uneven incorporation of xenocrysts (Sigmarsson et al., 1991; Bindeman et al., 2006). A notable exception is the 1996 Gjálp eruption of basaltic icelandite with identical isotope ratios as the Grímsvötn basalts (Sigmarsson et al., 2000). Beside major element concentration analyses on tephra glass by electron microprobe (EMP) in tens of tephra layers (Larsen et al., 1998), little is known about trace element concentrations and isotope ratios of Grímsvötn products. An exception is the Laki lava that has been extensively studied (e.g. Condomines et al., 1983; Sigmarsson et al., 1991; Kokfelt et al., 2006; Peate et al., 2010).

3 Sample collection and preparation

Tephra layers in outlet glaciers of Vatnajökull (Fig. 2) were collected either directly under the ice, corresponding to the winter snow after a given eruption and associated tephra fall, or by a small hand-driven ice corer (Larsen et al., 1998). The ice-conserved tephra are, in principle, less prone to alteration than those exposed to humic acid in soil sections. The tephra stratigraphy of each outlet glacier is established by combination of written eruption records, major element tephra glass analyses and by correlations to readily identifiable key tephra layers (Larsen et al., 1998). The composite Vatnajökull tephra record confirms the basaltic character of Grímsvötn magma since the late 12th century (oldest ice is approximately from AD 1200). An exception is the AD 1575 icelandite that together with the 1996 basaltic icelandite (from Gjálp) are the only evolved magma attributed to the volcano. This most evolved tephra layer is found on different outlet glaciers either together with a basaltic Grímsvötn tephra or as an individual layer. It is therefore suspected to be of Grímsvötn origin, however, the possibility of a contemporaneous eruption at a different volcano cannot be excluded.
Twenty tephra samples of the largest and coarsest tephra layers were selected from those of the outlet glaciers and dried. The samples represent tephra that fell within 40 km of the volcano. Two samples were collected from the 1455 tephra layer in a soil section 80 km SW of Grimsvötn, one by carefully handpicking the largest lapilli-sized fragments only (1455B) and the second as a bulk sample (1455C); both were collected for comparison purpose with ice-conserved tephra

(1455A). In addition, two lava samples together with a magmatic tephra from the Laki 1783-84 eruption (Sigmarsson et al., 1991) and a tephra from the 1996 Gjálp eruption (Sigmarsson et al., 2000) were included in this study for completeness.

4 Analytical methods

Electron-probe microanalysis (EPMA) of major-element concentrations in tephra glass allowed correlations of tephra layers from different outlet glaciers and the construction of composite tephra stratigraphy for the Vatnajökull ice-cap; these concentrations were also used to trace each layer to its volcano of origin (e.g. Larsen et al., 1998; Oladottir et al., 2011). The accelerating voltage was kept at 15 kV and the sample current at 10 nA during the EPMA, with 5-12 μm of glass surface excited.

4.1 Trace element concentrations

The expected limited variability in trace element concentrations demands high-precision analytical procedure. The concentrations were determined with an ICP-MS (Agilent 7500ce) at Laboratoire Magmas et Volcans in Clermont-Ferrand and are displayed in Table 1. Approximately 100 mg of rock powder were dissolved in a concentrated HF-HNO3 (4:1) mixture. Samples were then dried down, taken up in 7N HNO_3 and dried again. Digested samples were finally diluted ~ 4500 times in a mixture of HNO_3 2% - HF 0.05%, containing Be, Ge, In, Tm and Bi (10 ppb) as internal standards to monitor the instrumental drift. The BHVO-2 reference material was analyzed for external calibration (Chauvel et al., 2011). Three international reference materials (BCR-2, AGV-1 and BIR) were also analyzed (Table A.1). The results are generally within 3% of published values (e.g. Raczek et al., 2001; Willbold and Jochum, 2005; Chauvel et al., 2011). Precision is usually better than 5% (2σ level) for elements of the first transition series (Sc to Zn) and 2% for other elements. Eight samples were fully duplicated (Table A.1) and the relative difference between the duplicate samples is better than 2% for most elements.

4.2 Isotope ratios

Before HF-HNO_3 digestion, samples were leached with 0.5N HCl for 30 min in ultrasonic bath and washed for another 30 min in deionised water, in order to remove possible post-eruptive surface contamination. Lead was the first element isolated using the technique of Manhès et al. (1984) with two successive passes through Bio-Rad AG1-X8 resin. Both Sr and Nd were first collected with 0.7 HBr, while Pb was later eluted using 6N HCl. The dried HBr fractions were converted to chlorides and Sr and Nd isolated (Pin et al., 1994; Pin and Zalguedi, 1997. Total procedure blanks (n=8) have 20, 220 and 1100 pg of Pb, Nd and Sr, respectively, which is negligible relative to the amount of Pb (~ 0.15 μg), Nd (~ 3 μg) and Sr (~ 30 μg) processed.
Strontium and Nd isotope ratios were measured by Thermal Ionization Mass Spectrometry (TIMS; Thermo Finnigan Triton) and were normalized for mass

fractionation to $^{86}Sr/^{88}Sr=0.1194$ and $^{146}Nd/^{144}Nd=0.7219$. The NBS 987 Sr and JNdi-1 Nd standards were run regularly during the different analytical sessions and yielded an $^{87}Sr/^{86}Sr$ of 0.710237±10 (2σ, n=35) and a $^{143}Nd/^{144}Nd$ of 0.512105 ±13 (2σ, n=23), respectively. Lead isotope compositions were measured using two different mass spectrometers: a Nu Plasma 500 HR MC-ICP-MS at ENS (Lyon, France), and a Thermo Finnigan Neptune Plus MC-ICP-MS in Clermont-Ferrand. Both static mode and natural thallium addition technique (White et al., 2000) were used. The NBS 981 Pb standard was run every second or third sample and yielded mean values of $^{206}Pb/^{204}Pb$ = 16.9354 ±33 (2σ, n=25), $^{207}Pb/^{204}Pb$ = 15.4928 ±34 and $^{208}Pb/^{204}Pb$ = 36.6966 ±78 in Lyon and mean values of $^{206}Pb/^{204}Pb$ = 16.9475 ±18 (2σ, n=37), $^{207}Pb/^{204}Pb$ = 15.5072 ±21 and $^{208}Pb/^{204}Pb$ = 36.7471 ±56 in Clermont-Ferrand. Using the sample-standard bracketing technique, Pb isotope ratios were corrected to the NBS 981 TIMS triple spike values recommended by Galer and Abouchami (1998). In order to evaluate the potential instrumental bias between Pb isotope ratios measured on the Nu and Neptune mass spectrometers, three rocks were analysed on both instrument (using the same analyte) and the results agree within errors (Table 2).

International reference materials (BHVO-2, BCR-2 and AGV-1) were processed and analysed throughout the course of this study. For BHVO-2 and BCR-2, both leached (following the same procedure as for samples) and unleached powders were processed. Results are in good agreement with those previously published (e.g. Raczek et al., 2003; Weis et al. 2006; Chauvel et al., 2011; Pin et al., 2014). In addition, seven samples were fully duplicated and the external reproducibility of the isotope ratios is given in the footnote to Table 2.

5 Results

The bulk tephra from the soil section (sample #1455C not listed here) exhibit strange composition compared to that of all other tephra samples, most likely reflecting post-eruptive modification. Secondary processes, such as admixture of tephra and air blown fragments from the environment, possible bio-disturbance of small tephra grains and soil particles and/or humic acid percolation, most likely explain the peculiar composition of the bulk tephra sample. The implication that can be drawn from this composition on sampling procedures is beyond the scope of this paper and will be discussed elsewhere. A comparison from analysis of the two other tephra samples from the 1455 eruption reveals that tephra collected at location 80 km SW of the volcano (1455B) has significantly different trace element composition compared to that sampled on the glacier (1455A; Fig. 3), most likely due to mineral fractionation during aeolian transport of the tephra. These results demonstrate the importance of comparing the tephra whole-rock trace element concentrations only between tephra deposited at similar distance from the eruption crater.

5.1 Temporal variations

Incompatible trace element concentrations vary significantly as illustrated by Rb, Nb and Th concentrations (range: 6.01 – 9.20 ppm, 14.0 – 19.6 ppm, and 0.875-

1.34, respectively; Table 1). They display a striking correlation with the date of eruption (Fig. 4). The increase in Th concentrations by over 50% reflects its highly incompatible behaviour in the Grímsvötn basalt magma, allowing its use as a magma differentiation index. The evolved tephra (AD1575, icelandite, 1996 basaltic icelandite and the 1998 tholeiite) show relatively strong enrichment when normalized to the oldest and least evolved AD 1200 tephra (Fig. 5). In contrast, ratios between highly incompatible elements remain constant with the notable exception of the AD1575 and 1998 tephra. These two anomalous tephra also have lower concentrations of compatible elements such as Sc, as clearly revealed when temporal variations are examined (Fig. 6).

5.2 Ratios of trace elements and isotopes

The ratios between the most incompatible elements are surprisingly uniform: Th/U = 3.40 ±0.05 (1 SD), Rb/Th = 6.81 ±0.12 (1 SD), Rb/Cs = 93.1 ± 2.9 (1 SD), Ba/U = 258 ±3 (1 SD) and Nb/Th = 15.4 ±0.6 (1 SD). The standard deviation around the mean values is close to the estimated analytical uncertainty.

Variations of Sr-Nd isotope ratios are small in tephra produced over the last 8 centuries (Table 2) and indistinguishable from those of Sigmarsson et al. (2000). A notable exception is the AD 1575 icelandite with significantly higher $^{87}Sr/^{86}Sr$ and lower $^{143}Nd/^{144}Nd$ than the rest of the sample suite. The Pb isotope compositions are clustered at the enriched end of the NRZ linear array defined by Peate et al. (2010; Fig. 7 and 8). The AD 1575 icelandite has higher Pb isotope ratios, similar to those of the singular Öræfajökull volcano (Peate et al., 2010; Manning and Thirlwall, 2014; Fig. 1).

6 Discussion

6.1 Aeolian fractionation of trace element concentrations

Ratios of trace element concentrations in soil-kept tephra over those from the glacier are less than unity for the highly compatible elements Cr, Ni, Cu, Sc, Li, Sr an Co and the ratios increase in that order (Fig. 3). The minerals preferentially falling from the tephra cloud transported to the SW are those with the highest partition coefficient for the compatible elements, namely clinopyroxene and olivine. Less plagioclase is separated from the tephra on its way from the glacier to the soil section were the tephra was collected. This concurs with the density order clinopyroxene ~ olivine >> plagioclase. Negligible fractionation of FeTi-oxides occurred as demonstrated by V and Ti ratios being close to unity.

The preference for the melt phase over minerals, or incompatibility, appears to increase from HREE to MREE and LREE and HFSE (Heavy-, Middle- and Light Rare Earth Elements, and High-Field Strength Elements, respectively) although the ratios of these elements are all within error. The most incompatible elements are clearly those of Cs, U and Th. The Pb enrichment is noteworthy and likely represents an additional enrichment process. The limited enrichment of Ba may reflect its non-negligible incorporation in plagioclase. However, that of Rb cannot

be ascribed to potential mobility after deposition since Cs, which should behave similarly, is enriched by 12% comparable to that of U and Th as expected. In essence, the order in which the elements are enriched or depleted during aeolian transport is principally dictated by the bulk partition coefficients.

6.2 Fine-scale trace element variation with time

Trace element concentrations and their ratios show significant and regular temporal variations when five tephra are excluded, namely the AD 1223, 1345, 1532, 1575 and 1998 tephra (Fig. 5). The signification of these outliers is discussed further below. The remarkable linear increase over time of the incompatible trace element (e.g. Th, Ba, Nb) concentrations, and the contrasting decrease of those of compatible element (e.g. Sc and Ni), is systematic for the whole eruption period studied (from AD 1200 to AD 2011). These systematic temporal variations are associated with linear correlations between incompatible elements (Fig. 9) that can be used to evaluate the details of the magma differentiation processes.

The most incompatible elements (e.g. U, Rb, Cs) have best fit lines, when plotted against Th concentrations, passing through the origin as expected if fractional crystallization is the only magma differentiation process. Detailed examination reveals, however, that other elements considered as highly incompatible (e.g. Ba, Nb) have an intercept higher than nought. This could be taken (1) as an argument against the simple differentiation mechanism, or (2) that the fractionating crystal assemblage is composed of minerals with elevated partition coefficients (D) for these elements or (3) that their behaviour reflect a polybaric fractionation with changing D. Constant oxygen- (Bindeman et al., 2006) and radiogenic isotope ratios in Grímsvötn tephra, excepting the outliers defined above, strongly suggest co-genetic magma evolution without significant crustal input during the last eight centuries magma evolution. This does not eliminate magma mixing between basalts of slightly different compositions that would only diminish the spread observed in figure 9. The fractionating mineral composition is best derived from the rare crystals observed, namely plagioclase, olivine and clinopyroxene. These minerals are not known to have elevated D for incompatible elements (e.g. compilation available at www.EarthRef.org). The subtle change in slope for instance on Ba vs Th plot (Fig. 9) suggests that tephra with less thorium concentrations than 1.1 ppm have linear relationships passing through the origin, whereas those with higher concentrations plot on a line with lower slope and an intercept higher than 0. The more evolved magmas thus have higher D for Ba, most likely due to increasing plagioclase proportions in the fractionating assemblage. Indeed, plagioclase is known to incorporate small amounts of Ba. This suggests that the more evolved tephra resided in higher level magma chamber with enhanced plagioclase fractionation before eruption or that the liquid-line-of-descent of the tholeiites have reached cotectic configuration requesting less olivine compared to clinopyroxene in the crystallizing mineral assemblage. The latter possibility would require a deeper magma reservoir without recharging of more primitive basalts during the historical period.

In a similar way, inspection of the correlation between Nb and Th concentrations reveals a kink at Th ≥ 1.1 ppm. This may reflect increasing clinopyroxene proportions in the fractionating assemblage. Clinopyroxene may have non-negligible D_{Nb}, which has been determined experimentally and calculated, respectively, as high as 0.24 and 1.24 (Bennett et al., 2004; Johnson and Schwab, 2004). Another possibility is that the onset of FeTi-oxide, with elevated D_{Nb}, crystallization starts at Th equal or higher than 1.1 ppm. Indirectly, this would imply subtle variations in fO_2 conditions in the magma plumbing system; perhaps higher fO_2 closer to the shallow hydrothermal system. These possibilities readily account for the fine change in slopes on element versus Th concentration diagrams (Fig. 9) and the variable Th/Nb in figure 6.

The negative correlations of the compatible elements Cr and Ni with Th in figure 10 concurs with the idea of polybaric fractionation during which, for instance, less clinopyroxene fractionated from the magma erupted in 2011 compared to those forming the general trend. Moreover, the steeper decrease in Cr compared with Ni points to dominating role of clinopyroxene fractionation compared to that of olivine in the evolved tholeiites. Similar explanation can be advanced for the irregular decrease of Sc and Sr with increasing Th concentrations.

It is worth noting that the large fissure eruption of Laki (AD 1783-84) produced magma with Th concentrations ranging from 1.08 to 1.16 ppm (Sigmarsson et al., 1991), exactly the composition where a change in slope occurs in figure 9. This suggests a direct effect of the Laki eruption upon the magma system beneath Grímsvötn volcanic system.

The five outliers plot above the main trend in the Th, Ba, Nb, La/Sm, Rb/Yb and Th/Nb vs. time plots (Fig. 6), with AD 1575 icelandite showing the most extreme incompatible trace element enrichment. Their composition is not explained by quasi-closed system behaviour.

6.3 Fine-scale Pb isotope ratio variations in Grímsvötn magmas

Most of the tephra plot along the NRZ array of Peate et al. (2010) in Pb-Pb isotope diagrams (Fig. 7). Two of the "outliers", with enriched trace element contents, AD 1223 and 1998, have similar Pb isotope ratios as the bulk of the tephra suite. The other three (AD 1345, 1532 and 1575) plot above the NRZ arrays close to Holocene basalts from the Sída district (Sigmarsson and Carpentier, 2015), a little SE of the Laki eruption fissure (Fig. 1), and form a linear array between Öræfajökull magma and Grímsvötn basalts (Fig. 8). The AD 1575 icelandite plots at the enriched end of this array and has an isotope composition indistinguishable from those of Öræfajökull volcanics. Similar relationship is observed in the La/Sm vs. $^{208}Pb/^{204}Pb$ plot (Fig. 11), where most tephra plot on a binary mixing curve between those of AD 1575 and AD 1200.

6.4 Signification of "outliers"

The G-1223 tephra has same isotope ratios as other tephra but relatively high concentrations of incompatible elements suggesting relatively enhanced magma

evolution in perhaps in an isolated magma pocket from the main magma supply. The G-1998 tephra requires somewhat similar explanation. In marked contrast, the G-1345, -1532 and -1575 tephra are characterized by an "Öræfajökull type" component and might be associated with the Thordarhyrna volcanic system together with the Síða Holocene basalt lavas; details of which will be discussed elsewhere. Influence of this component on Grímsvötn magmas after AD 1783-84 Laki fissure eruptions is, however, not detected.

6.5 New constraints on Grímsvötn magmatic system

The linear increase in incompatible element concentrations suggests semi-closed system magma chamber (no input of new magma, only output of increasingly differentiated basalt) at depth. The decreasing melt fraction, F, since AD 1200 can be simply estimated from the Rayleigh law, $C = C_0 \times F^{(D-1)}$, where C and C_0 are, respectively, the element concentrations at a given time and initially (AD 1200) and D the bulk partition coefficient between fractionating crystals and melt. The D^{Th} is negligible for olivine, clinopyroxene and plagioclase fractionating at Grímsvötn and can be considered close to 0. Over the last 8 centuries, the melt fraction of the magma reservoir beneath Grímsvötn has decreased by 35% according to the Th concentration of the 2011 tephra. The magma production rate of Grímsvötn is poorly known. However, the volume of its 20th century eruptions has been estimated at about 0.9-1.0 km^3 (Gudmundsson, 2005). By considering the last 100 years, taking into account the two most recent eruptions, the relatively small 2004 eruption (DRE volume of 0.02 km^3, Jude-Eton et al., 2012) and the large 2011 eruption (DRE of 0.25 km^3, Hreinsdóttir et al., 2014), the erupted volume is 1.2 km^3. The level of activity of the central volcano has remained similar over the last 800 years (Larsen et al., 1998), indicating that a constant production rate of 1 km^3 per century is a reasonable value. Thus, the minimum volume of melt in the magma reservoir must have been 8 km^3/0.35 = 23 km^3.

The volume of magma produced in eruptions at Grímsvötn, typical range 0.02-0.25 km^3, is close to 0.1-1% of the estimated ~20 km^3 magma reservoir extending to 3 km below the surface by Alfaro et al (2007). This is in line with what is inferred for magma chambers ruptured by overpressure generated by exsolution of a gas phase at shallow depth (Tait et al, 1989). Moreover, these considerations also support the assumption of an elastic behaviour of the upper crust in which the magma chamber is located; an assumption frequently used in geodetic data inversions (e.g. Reverso et al., 2014).

A deep magma reservoir with a residence time in the range of 100 to 1000 years was inferred from homogeneously low oxygen isotope ratios in historical Grímsvötn glass, oxygen and trace-elements-in-minerals diffusion time-scales and ^{238}U-series disequilibria (Bindeman et al., 2006). This deep reservoir feeds the crustal magmatic system where the magma may occasionally pass through a dike and sill complex in cooler parts of the system. The consequence of the latter is faster magma differentiation and the divergence (G1223 and G1998) from the observed regular temporal variations in the tephra composition.

6.6 Volume of magma under Grímsvötn evaluated from eruptions and heat-flow estimates

The volume of crystallizing magma beneath Grímsvötn can be estimated from the heat flux liberated. Quantification of heat-flow from active volcanoes is impossible in most cases. At Grímsvötn volcano the subglacial lake results from geothermal heat that melts the glacier providing a natural calorimeter if the ice melting can be estimated (Björnsson et al., 1982; Björnsson and Gudmundsson, 1993). A floating ice-lid on top of the lake is lifted semi-periodically when the lake water is released by flow along the glacier bed (e.g. Björnsson, 2003). The thermal energy (E_t) liberated over the period 1922-1991 was evaluated by Björnsson and Gudmundsson (1993) on the basis of subglacial melting as $(8.1\pm1.6)\cdot10^{18}$ J, whereof about 20% is the result of direct melting of ice in eruptions, and 80% from solidification and cooling of magma in the crust. This gives a heat release through geothermal activity (excluding erupted magma) of about 10^{19} J over 100 years. Assuming a similar heat-flux for the last 8 centuries, the volume of consolidating basaltic magma (V_m) can be calculated from the following relationship:

$$V_m = E_t / (\rho \times (L + c_p (T_{init} - T_{final}))),$$

where ρ is magma density, L denote the latent heat of crystallization, and c_p heat capacity of the basalt. The magma density for Grímsvötn qz-tholeiite is 2750 kg/m^3, the L is approximately 400 kJ/kg (Lange et al., 1994; Bouhifd et al., 2007; Sigmarsson et al., 2013) and the average specific heat capacity as measured for Grímsvötn basalts between 0°-1130°C, c_p, is close to 1.25 kJ/kg °C (Gudmundsson et al., 2009). Taking into account the temperature dependency of enthalpy of crystallization has only small effect on the volume calculation. The initial temperature (T_{init}) will be close to the liquidus of basaltic magma, or approximately 1200 °C. A lower bound on the final temperature (T_{final}) could be as low as 200 °C (Björnsson et al., 1982), here referred to as Case A, or simply close to the magma solidus (ca. 900 °C - Case B). For the higher temperature drop ΔT = 1000 °C, the heat released is by solidification and cooling is 1400 kJ/kg, or $3.9\cdot10^{18}$ J/km^3, using the same magma density as before. For ΔT = 300 °C the corresponding values are 800 kJ/kg, or $2.2\cdot10^{18}$ J/km^3. The lower final temperature is probably too low but may be closer to the actual case, since the transient behaviour of the power output indicates that solidification and cooling of shallow intrusions are a significant source for these unusually high heat output values (Björnsson and Gudmundsson, 1993).

The very high heat flux observed at Grímsvötn are unlikely to have been sustained at 10^{19} J/century (3 GW) for the last 800 years. However, the occurrence of frequent jökulhlaups is well documented since 1600 AD but more uncertainty exists regarding the period 1200-1600 (Thorarinsson, 1974). Thus, a lower bound of geothermal heat release is used here, namely a value of $3\cdot10^{18}$ J per century (1 GW).

The results obtained for the volumes of magma erupted and solidified in the crust over the last 800 years are given in Table 3. By combining the volume

490 erupted in Grímsvötn, Laki 1783-4 and the estimates for the magma crystallized
491 in the crust, we obtain an estimate of the total magma solidified and hence an
492 estimate of the volume of the whole system 800 years ago. Using 35% reduction
493 in magma volume over the last 8 centuries, the initial magma volume is obtained
494 for the whole system as 80-217 km^3. However, the highest value of 217 km^3 is
495 considered unlikely, since as previously stated the data from the 20th century
496 require a large component from shallow intrusions (Björnsson and
497 Gudmundsson, 1993), which cannot be reconciled with a model assuming
498 cooling only to the solidus. The results therefore indicate an initial magma
499 volume of about 100 km^3 (80-134 km^3) 8 centuries ago, and the volume at
500 present being 52-87 km^3.
501
502 This value for magma in the system can be compared with the volume of basic
503 intrusives inferred under Grímsvötn from gravimetry, being about 400 km^3
504 above 5-6 km depth in the crust (Gudmundsson and Milsom, 1997), similar to
505 that of other large central volcanoes in the region (Gudmundsson and
506 Högnadóttir, 2007). Our results do not contradict these data, as they only require
507 a small fraction (max. ~10%) of the crust under the volcano to be in molten
508 state.
509
510 Seismic studies of Grímsvötn (Alfaro et al., 2007) indicate the presence of melt at
511 two depths under Grímsvötn, at or above 3 km and at 5-7 km. Constraints on the
512 shape or thickness of especially the lower body are, however, not strict. These
513 bodies combined, possibly extending to a greater depth may constitute the
514 present magma system under Grímsvötn. An alternative model would be a more
515 widespread region of partial melt in the lower crust or at the crust-mantle
516 boundary. If such a body were to underlie both Grímsvötn and the fissure swarm
517 extending to Laki, it would be 75 km long. A body of this nature containing 20-50
518 km^3 of magma and possibly 0.1-0.3 km thick would not contradict our data. If
519 such a body exists it is likely that it would give rise to seismic reflections
520 analogous to those seen at some mid ocean ridges (Marjanović, et al. 2014).
521 Seismic and possibly deformation studies should help in differentiate between
522 these two contrasting geometries of the Grímsvötn magma system.
523
524
525 *6.7 Magmatic differentiation rates*
526
527 Over the last 8 centuries, the melt fraction of the deep magma reservoir having
528 decreased by 35% corresponds to a differentiation rate of 0.35/800 yrs, or 4 x
529 10^{-4} yr^{-1}. Magma differentiation rates have been argued to be similar (Blake and
530 Rogers, 2005) for tholeiitic basalt from Ardoukoba, Djibouti, MORB from the East
531 Pacific Rise, alkali basalt to mugearite from Vestmannaeyjar, Iceland, and basaltic
532 andesites from Miyakejima, Izu–Bonin arc. In all cases ($^{226}Ra/^{230}Th$) activity ratio
533 correlates with indices of fractional crystallization, such as Th (Vigier et al., 1999;
534 Sims et al., 2003; Sigmarsson, 1996; Yokoyama et al., 2003), and if the decreasing
535 ($^{226}Ra/^{230}Th$) is only caused by simultaneous fractional crystallization and
536 ageing of magma it would be consistent with constant fractional crystallization
537 rate of 2 to 6 × 10^{-4} yr^{-1}. This is a surprisingly similar rate to that determined in
538 a very different manner for Grímsvötn. Moreover, such a similarity would

indicate a universal differentiation rate despite variable geodynamic context of these different volcanoes, and consequently variable thermal regime. However, the Ra partition coefficient assumed by Blake and Rogers (2005) is an order of magnitude lower than that calculated from the basalt-hawaiite-mugearite evolution at Vestmannaeyjar (Sigmarsson, 1996) and that determined experimentally (Fabrizzo et al., 2009). Moreover, if large ^{210}Pb deficit in Vestmannaeyjar magma is to be explained by degassing as suggested by (Blake and Rogers, 2005) several decades of degassing time would be required from a closed-system magma chamber before the Surtsey and Heimaey eruptions (and that of Ardoukoba, Djibouti), which appears unrealistic. The likelihood of long term degassing before eruption for the MORB from the East Pacific Rise and basaltic andesites from Miyakejima, Izu–Bonin arc cannot be evaluated due to lack of ^{210}Pb-^{226}Ra disequilibrium data. In any case, pre-eruptive degassing would lower the magmatic pressure at depth and thus could be expected to lower the likelihood of an ensuing eruption.

A more realistic estimate of magma differentiation rate at Vestmannaeyjar can be estimated from the 10 years differentiation time (Sigmarsson 1996) that are two orders of magnitude faster than that of Grímsvötn, or 4×10^{-2} yr^{-1}. This difference is readily explained by different crustal thermal state and thus magma chamber power output (cooling). The islands of Vestmannaeyjar are the surface manifestation of an embryonic volcanic system constructed at the tip of a propagating rift through a cold crust (geothermal gradient even too low for house heating!), whereas Grímsvötn, the most active volcanic system of Iceland, is located above the core of the Iceland mantle plume. The high magma flux from the mantle plume and the consequent steep geothermal gradient lead to significantly hotter crustal environment and less efficient heat loss from incoming basalts that most likely causes the slow magma differentiation rate at Grímsvötn compared with Vestmannaeyjar.

6.8 Possible future activity of Grímsvötn volcano

The rate of increasing incompatible element concentrations permits exploring possible future scenario assuming that the magmatic system beneath the volcano follows the established historical evolution. Without magma recharge and if the deep magma reservoir beneath Grímsvötn differentiates at the same rate, then its lifetime will be close to 2300 yrs. The linear increase in e.g. Th concentration suggests that the volcano is likely to principally produce basalts for the next 500-1000 years. Evolution of water concentration will most likely follow those of incompatible elements with consequent increases in potential explosiveness of future Grímsvötn magma.

7 Conclusions

1 - Historical Grímsvötn tephra show small but significant and variations in trace element concentrations and isotope ratios.
2 - Regular increase in incompatible element concentrations suggests that a principal magma reservoir has been active over the historical period.

3 – The liquid fraction of this reservoir has decreased by 35% over the last eight centuries.
4 – The actual volume of magma in the reservoir is considered to be 50-90 km^3.
5 – Magma differentiation rates are slow and close to 4×10^{-4} yrs^{-1}.
6 - The increasing magma evolution could lead to enhanced explosiveness of the Grímsvötn basalt in the future.

Acknowledgement

Samples of this study were collected with aid from the Glaciological Society of Iceland. Expert technical assistance was given by Chantal Bosq (chemistry), Jean-Luc Piro (ICP-MS) and Abdel-Mouhcine Gannoun (MC-ICP-MS). M.C. was supported by the "ClerVolc labex" project of the French Government. A grant from the Iceland Science Fund "Volcano Anatomy" and the European Community "Futurevolc" projects financed the analytical cost. All this is gratefully acknowledged. This is a ClerVolc contribution #XXX.

References

Albarède, F. 1993. Residence time analysis of geochemical fluctuations in volcanic series. Geochim. Cosmochim. Acta 57, 615-621.

Alfaro, R., Brandsdóttir, B, Rowlands, D.P., White, R.S., Gudmundsson, M.T., 2007. Structure of the Grímsvötn central volcano under the Vatnajökull icecap, Iceland. Geophys. J. Int. 168, 863-876.

Bennett, S., Blundy, J., Elliott, J., 2004. The effect of sodium and titanium on crystal-melt partitioning of trace elements. Geochim. Cosmochim. Acta 68, 2,335-2,347. doi: 10.1016/j.gca.2003.11.006.

Bindeman, I., Sigmarsson, O., Eiler, J., 2006. Time constraints on the origin of large volume basalts derived from O-isotopes and trace element mineral zoning and U-series disequilibria in the: Laki and Grímsvötn volcanic system. Earth Planet. Sci. Let. 245, 245–259.

Björnsson, H., Björnsson, S., Sigurgeirsson, Th., 1982. Penetration of water into hot rock boundaries of magma at Grímsvötn. Nature 295, 580-581.

Björnsson, H., Guðmundsson, M.T., 1993. Variations in the thermal output of the subglacial Grímsvötn Caldera, Iceland. Geophys. Res. Lett. 20, 2127-2130.

Björnsson, H., 2003. Subglacial lakes and jökulhlaups in Iceland. Global and Planetary Change 35, 255-271.

Blake, S., Rogers, N., 2005. Magma differentiation rates from (226Ra/230Th) and the size and power output of magma chambers. Earth Planet. Sci. Lett. 236, 654–669.

637 Bouhifd, M.A., Besson, P., Courtial, P., Gérardin, C., Navrotsky, A., Richet, P., 2007.
638 Thermochemistry and melting properties of basalt. Contrib. Min. Petrol. 153,
639 689-698.
640
641 Carpentier, M., Sigmarsson, O., 2015. Tectonic control on basalt compositions in
642 Iceland. G-cube; submitted manuscript.
643
644 Chauvel, C., Bureau, S. and Poggi, C., 2011. Comprehensive chemical and isotopic
645 analyses of basalt and sediment reference materials. Geostandards and
646 Geoanalytical Research 35, 125-143.
647
648 Condomines, M., Gronvold, K., Hooker, P. J., Muehlenbaehs, K., O'Nions, R. K.,
649 Oskarsson, N., Oxburgh, E. R., 1983. Helium, oxygen, strontium and neodymium
650 isotopic relations in Icelandic volcanics. Earth Planet. Sci. Lett. 66, 125-36.
651
652 Fabbrizio, A., Schmidt, M. W., Günther, D., Eikenberg, J., 2009. Experimental
653 determination of Ra mineral/melt partitioning for feldspars and 226Ra-
654 disequilibrium crystallization ages of plagioclase and alkali-feldspar. Earth
655 Planet. Sci. Lett. 280, 137-148.
656
657 Galer, S.J.G., Abouchami, W., 1998. Practical application of lead triple spiking for
658 correction of instrumental mass discrimination. Mineralogical Magazine 62A,
659 491-492.
660
661 Gudmundsson, M.T., Björnsson, H. Pálsson, F., 1995. Changes in jökulhlaup sizes
662 in Grímsvötn, Vatnajökull, Iceland, 1934-1991, deduced from in situ
663 measurements of subglacial lake volume. J. Glaciol. 41, 263-272.
664
665 Gudmundsson, M.T. and J. Milsom., 1997. Gravity and magnetic studies of the
666 subglacial Grímsvötn volcano, Iceland. Implications for crustal and thermal
667 structure. J. Geophys. Res. 102, 7691-7704.
668
669 Gudmundsson, M.T., 2005. Subglacial volcanic activity in Iceland. In: Caseldine,
670 C., Russel, A. Hardardóttir, J., Knudsen, Ó. (Eds): Iceland - Modern processes and
671 past environments. Developments in Quaternary Science 5, Elsevier, 127-151.
672
673 Gudmundsson, M.T., Högnadóttir, T. 2007. Volcanic systems and calderas in the
674 Vatnajökull region, central Iceland, constraints on crustal structure from gravity
675 data. Journal of Geodynamics 43, 153-169.
676
677 Hreinsdóttir, S., Sigmundsson, F., Roberts, M., Björnsson, H., Grapenthin, R.,
678 Arason, P., Árnadóttir, Th., Hólmjárn, J., Geirsson, H., Bennett, R. A.,
679 Guðmundsson, M. T., Oddsson, B., Ófeigsson, B. G., Villemin, T., Jónsson, Th.,
680 Sturkell, E., Höskuldsson, Á., Larsen, G., Thordarson, Th., Óladóttir, B. A., 2014.
681 Volcanic plume height correlated with magma pressure change at Grímsvötn
682 volcano, Iceland, Nature Geoscience, DOI: 10.1038/NGEO2044.
683
684 Johnson, A., Schwab, B., 2004. Constrainst on clinopyroxene/melt partitioning

685 REE, Rb, Sr, Ti, Cr, Zr, and Nb during mantle melting: First insights from direct
686 peridotite melting experiments at 1.0 GPa . Geochim. Cosmochim. Acta 68, 4,949-
687 4,962. doi: 10.1016/j.gca.2004.06.009.
688
689 Jude-Eton, T. C ., Thordarson, T., Gudmundsson, M.T., Oddsson, B., 2012.
690 Dynamics, stratigraphy and proximal dispersal of supraglacial tephra during the
691 ice-confined 2004 eruption at Grímsvötn Volcano, Iceland. Bull. Volc. 74, 1057-
692 1082.
693
694 Kokfelt, T., Hoernle, K., Hauff, F., Fiebig, J., Werner, R., Garbe-Schönberg, C. D.,
695 2006. Combined Trace Element and Pb-Nd-Sr-O Isotope Evidence for Recycled
696 Oceanic Crust (Upper and Lower) in the Iceland Mantle Plume J. Petrol. 47, 1705-
697 1749.
698
699 Lange, R.A., Cashman, K.V., Navrotsky, A., 1994. Direct measurements of latent
700 heat during crystallization and melting of ugandite and an olivine basalt. Contrib.
701 Min. Petrol. 118, 169-181.
702
703 Larsen, G., Guðmundsson, M.T., Björnsson, H., 1998. Eight centuries of periodic
704 volcanism at the center of the Iceland hotspot revealed by glacier
705 tephrostratigraphy. Geology 26, 943-946.
706
707 Manhès, G., Allègre, C.J., Provost, A., 1984. U-Th-Pb systematics of the eucrite
708 "Juvinas": precise age determination and evidence for exotic lead. Geochimica et
709 Cosmochimica Acta 48, 2247-2264.
710
711 Manning C.J.**,** Thirlwall M.F., 2014. Isotopic evidence for interaction between
712 Öraefajökull mantle and the Eastern Rift Zone, Iceland. Contrib. Min. Petro. 167,
713 959.
714
715 Marjanović, M., Suzanne M. Carbotte, S.M., Carton, H., Mladen R. Nedimović, M.R.,
716 Mutter, J.C., Canales, J.P. 2014. Multi-sill magma plumbing system beneath the
717 axis of the East Pacific Rise. Nature Geoscience 7, 825-829.
718
719 Oladottir, B., Larsen, G., Thordarson, T., Sigmarsson, O., 2005. Eruption frequency
720 of Katla volcano during the Holocene. Jökull 55, 53-74.
721
722 Oladottir, B., Larsen, G., Sigmarsson, O., 2011. Holocene volcanic activity at
723 Grímsvötn, Bárdarbunga and Kverkfjöll subglacial centres beneath Vatnajökull,
724 Iceland. Bull. Volcanol. 73, 1187–1208.
725
726 Peate, D.W., Breddam, K., Baker, J.A., Kurz, M.D., Barker, A.K., Prestvik, T.,
727 Grassineau, N., A.C., 2010. Compositional characteristics and spatial distribution
728 of enriched Icelandic mantle components. J. Petrol. 51, 1447-1475.
729
730 Peate, D.W., Baker, J.A., Jakobsson, S.P., Waight, T.E., Kent, A.J.R., Grassineau, N.V.,
731 Skovgaard, A.C. 2009. Historic magmatism on the Reykjanes Peninsula, Iceland: a
732 snap-shot of melt generation at a ridge segment. Contrib. Min. Petro. 157, p. 359-
733 383.

Pietruszka, A.J., Garcia, M.O., 1999. The size and shape of Kilauea Volcano's summit magma storage reservoir: a geochemical probe. Earth Planet. Sci. Lett. 167, 311-320.

Pin, C., Gannoun, A., Dupont, A., 2014. Rapid, simultaneous separation of Sr, Pb, and Nd by extraction chromatography prior to isotope ratios determination by TIMS and MC-ICP-MS. Journal of Analytical Atomic Spectrometry 29, 1858-1870.

Pin, C., Zalduegui, J.F.S., 1997. Sequential separation of light rare-earth element, thorium and uranium by miniaturized extraction chromatography: Application to isotopic analyses of silicate rocks. Analytica Chimica Acta 339, 79-89.

Pin, C., Briot, D., Bassin, C., Poitrasson, F., 1994. Contaminant separation of strontium and samarium-neodymium for isotopic analysis in silicate samples, based on specific extraction chromatography. Analytica Chimica Acta 298, 209-217.

Prestvik T., Goldber, S., Karlsson, H., Grönvold, K., 2001. Anomalous strontium and lead isotope signatures in the off-rift Öraefajökull central volcano in south-east Iceland evidence for enriched endmembers(s) of the Iceland mantle plume. Earth Planet. Sci. Lett. 190, 211-220.

Raczek, I., Jochum, K.P., Hofmann, A.W., 2003. Neodymium and strontium isotope data for USGS reference materials BCR-1, BCR-2, BHVO-1, BHVO-2, AGV-1, AGV-2F GSP-1, GSP-2 and eight MPI-DING reference glasses. Geostandards Newsletter: The Journal of Geostandards and Geoanalysis 27, 173–179.

Raczek, I., Stoll, B., Hofmann, A.W., Jochum, K.P., 2001. High-precision trace element data for USGS reference materials BCR-1, BCR-2, BHVO-1, BHVO-2, AGV-1, AGV-2, DTS-1, DTS-2, GSP-1 and GSP-2 by ID-TIMS and MIC-SSMS. Geostandards Newsletter 25, 77-86.

Reverso, T., Vandemeulebrouck, J., Jouanne, F., Pinel, V. Villemin, T., Sturkell, E., Bascou, P., 2014. A two-magma chamber model as a source of deformation at Grímsvötn Volcano, Iceland. J. Geophys. Res. 119, 4666- 4683. doi:10.1002/2013JB010569.

Sims, K.W.W., Goldstein, S.J., Blichert-Toft, J., Perfitt, M.R., Kelemen, P., Fornari, D.J., Michael, P., Murrell, M.T., Hart, S.R., DePaolo, D.J., Layne, G., Ball, L., Jull, M., Bender, J., 2002. Chemical constraints on the generation and transport of magma beneath the East Pacific Rise. Geochim. Cosmochim. Acta 66, 3481–3504.

Sigmarsson, O., Condomines, M., Grönvold, K., Thordarson, Th., 1991., Extreme magma homogeneity in the 1783-84 Laki eruption: origin of a large volume of evolved basalt in Iceland. Geophys. Res. Lett. 18, 2229-2232.

Sigmarsson, O., 1996. Short magma chamber residence time at an Icelandic volcano inferred from U-series disequilibria. Nature 382, 440-442.

Sigmarsson, O., Karlsson, H., Larsen, G., 2000: The 1996 and 1998 subglacial eruptions beneath Vatnajökull glacier in Iceland: contrasting geochemical and geophysical inferences on magma migration. Bull. Volc. 61, 468-476.

Sigmarsson, O., Condomines, M., Bachèlery, P., 2005. Magma residence time beneath the Piton de la Fournaise volcano, Reunion Island. Earth Planet. Sci. Lett. 234, 223-234.

Sigmarsson, O., Haddadi, B., Carn, S. Moune, S., Gudnason, J., Yang, K., Clarisse, L., 2013. The sulfur budget of the 2011 Grímsvötn eruption, Iceland. Geophys. Res. Lett. 40, 1–6, doi:10.1002/2013GL057760.

Tait, S., Jaupart, C., Vergniolle, S., 1989. Pressure, gas content and eruption periodicity of a shallow, crystallizing magma chamber. Earth Planet. Sci. Lett. 115, 107-123.

Thirlwall M.F., Gee, M.A.M.,Taylor, R.N., Murton, B.J., 2004. Mantle components in Iceland and adjacent ridges investigated using double-spike Pb isotope ratios. Geoch. Cosmoch. Acta 68, 361-386.

Thorarinsson, S., 1974. Vötnin stríð: saga Skeiðarárhlaupa og Grímsvatnagosa (Swift flowing rivers: the history of Grímsvötn jökulhlaups and eruptions). Menningarsjóður, Reykjavik, 254 pages.

Thordarson T., Self S., 1993. The Laki (Skaftar Fires) and Grimsvotn eruptions in 1783-1785. Bull. Volcanol. 55, 233-263.

Vigier, N., Bourdon, B., Joron, J.L., Allègre, C.J., 1999. U-decay series and trace element systematics in the 1978 eruption of Ardoukoba, Asal rift: timescale of magma crystallization. Earth Planet. Sci. Lett. 174, 81–97.

Yokoyama, T., Kobayashi, K., Kuritani, T., Nakamura, E., 2003. Mantle metasomatism and rapid ascent of slab components beneath island arcs: evidence from ^{238}U–^{230}Th–^{226}Ra disequilibria of Miyakejima volcano, Izu arc, Japan. J. Geophys. Res. 108, DOI: 10.1029/2002JB002103.

Weis, D., Kieffer, B., Maerschalk, C., Barling, J., de Jong, J., Williams, G.A., Hanano, D., Pretorius, W., Mattielli, N., Scoates, J. S., Goolaerts, A., Friedman, R.M., Mahoney, J.B., 2006. High-precision isotopic characterization of USGS reference materials by TIMS ans MC-ICP-MS. Geochemistry Geophysics Geosystems**,** 7: Q08006, doi:10.1029/2006GC001283.

White, W.M., Albarède, F., Télouk, P., 2000. High-precision analysis of Pb isotope ratios by multi-collector ICP-MS. Chemical Geology 167, 257-270.

Willbold, M., Jochum, K.P., 2005. Multi-element isotope dilution sector field ICP-MS: A precise technique for the analysis of geological materials and its application to geological reference material Geostandards and Geoanalytical Research 29, 63-82.

Figure Legends

Fig. 1 Map of Iceland showing the Neovolcanic zones and the locations of Grímsvötn, the Laki crater row and Öræfajökull volcano.

Fig.2 Tephra layer (G1823) being exposed in the ablation region of one of the outlet glaciers (Skeiðarárjökull) of Vatnajökull ice-cap.

Fig. 3 Comparison of two analysis of the 1455 tephra. One sample was collected from the glacier close to the volcano whereas the other one is lapilli-sized fragments from a soil section approximately 80 km SW of the volcano. Aeolian mineral fractionation dominated by early clinopyroxene and olivine fall-out during the tephra transportation causes the divergence from unity (see text for further discussion).

Fig. 4 Rubidium concentrations in historical Grímsvötn tephra as a function of their eruption year. Anomalous values are indicated by vertical stippled lines. See text for further discussion.

Fig. 5 Normalized trace element concentrations in Grímsvötn tephra to that of the oldest and least evolved basalt of the AD1200 tephra exposing anomalous samples. Depletion in Ba, Sr and Eu characterize the fractionation of plagioclase. Note the linear y-scale.

Fig. 6 Variations of several trace element abundances and trace element ratios in historical Grímsvötn tephra with age.

Fig.7 Lead-lead isotope diagram showing the new high precision data obtained for Grímsvötn tephra and basalts from Síða district. Published Pb data are from Thirlwall et al. (2004), Peate et al. (2009; 2010) and Manning and Thirlwall (2014). NRZ and SIVZ arrays as defined by Peate et al. (2010).

Fig. 8 Enlarged Pb-Pb isotope diagrams. Tephra with trace element composition outside the general temporal trend (Fig. 4 and 6) are highlighted. The Öræfajökull compositions are from Peate et al. (2010) and Manning and Thirlwall (2014)

Fig. 9. Linear correlation of nominally highly incompatible trace element concentrations with those of Th. The inflection point at ~1.1 ppm Th suggests a changing mineral fractionating assemblage (see text for further discussion).

Fig. 10 Decreasing concentrations of compatible elements with increasing Th concentrations. Melt evolution from fractional crystallization is shown for different partition coefficients. Changing mineral proportions in the fractionating assemblage explains the data scatter around the melt-evolution curves with variable D^{Sr}. Less plagioclase fractionation causes bulk D^{Sr} lower than unity and thus slight increase in Sr concentrations as a function of that of Th (see text for further discussion).

Fig. 11 Ratio of La over Sm vs $^{208}Pb/^{204}Pb$. Öræfajökull compositions from Prestvik et al. (2001), Peate et al. (2010) and Manning and Thirlwall (2014). A binary mixing curve between the tholeiites of Grímsvötn and a component close to the composition of Öræfajökull accounts tephra with anomalous composition in Fig. 4 and 6 (" the outliers") as well as most of the Síða district basalts (Sigmarsson and Carpentier, 2015). The higher La/Sm in the 1998 tephra suggests unidentified additional contribution.

Table Captions

Table 1 Trace element concentrations in Grímsvötn volcanic products.

Table 2 Isotope ratios of Sr, Nd and Pb in products of Grímsvötn volcanic system.

Table 3 Grímsvötn system since 1200 AD: estimates of magma erupted and solidified in the crust and the initial magma volume 800 years ago.

***Highlights (for review)**

1 - Historical Grímsvötn tephra show small but significant and variations in trace element concentrations and isotope ratios.
2 - Regular increase in incompatible element concentrations suggests that a principal magma reservoir has been active over the historical period.
3 – The liquid fraction of this reservoir has decreased by 35% over the last eight centuries.
4 – The actual volume of magma in the reservoir is considered to be 50-90 km^3.
5 – Magma differentiation rates are slow and close to 4×10^{-4} yrs^{-1}.
6 - The increasing magma evolution could lead to enhanced explosiveness of the Grímsvötn basalt in the future.

Figure
Click here to download high resolution image

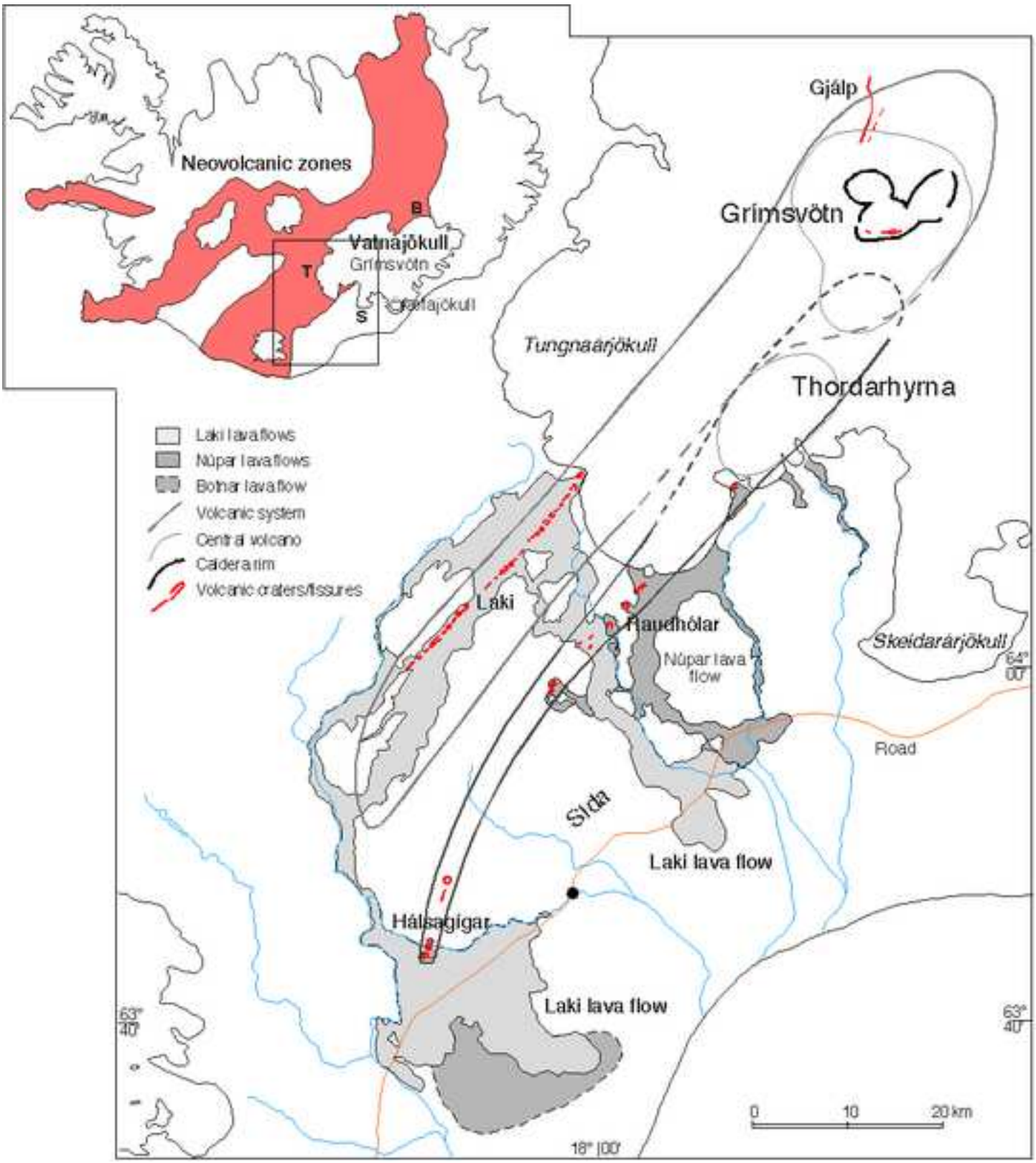

Figure

Click here to download high resolution image

Figure
Click here to download Figure: Fig. 3.pdf

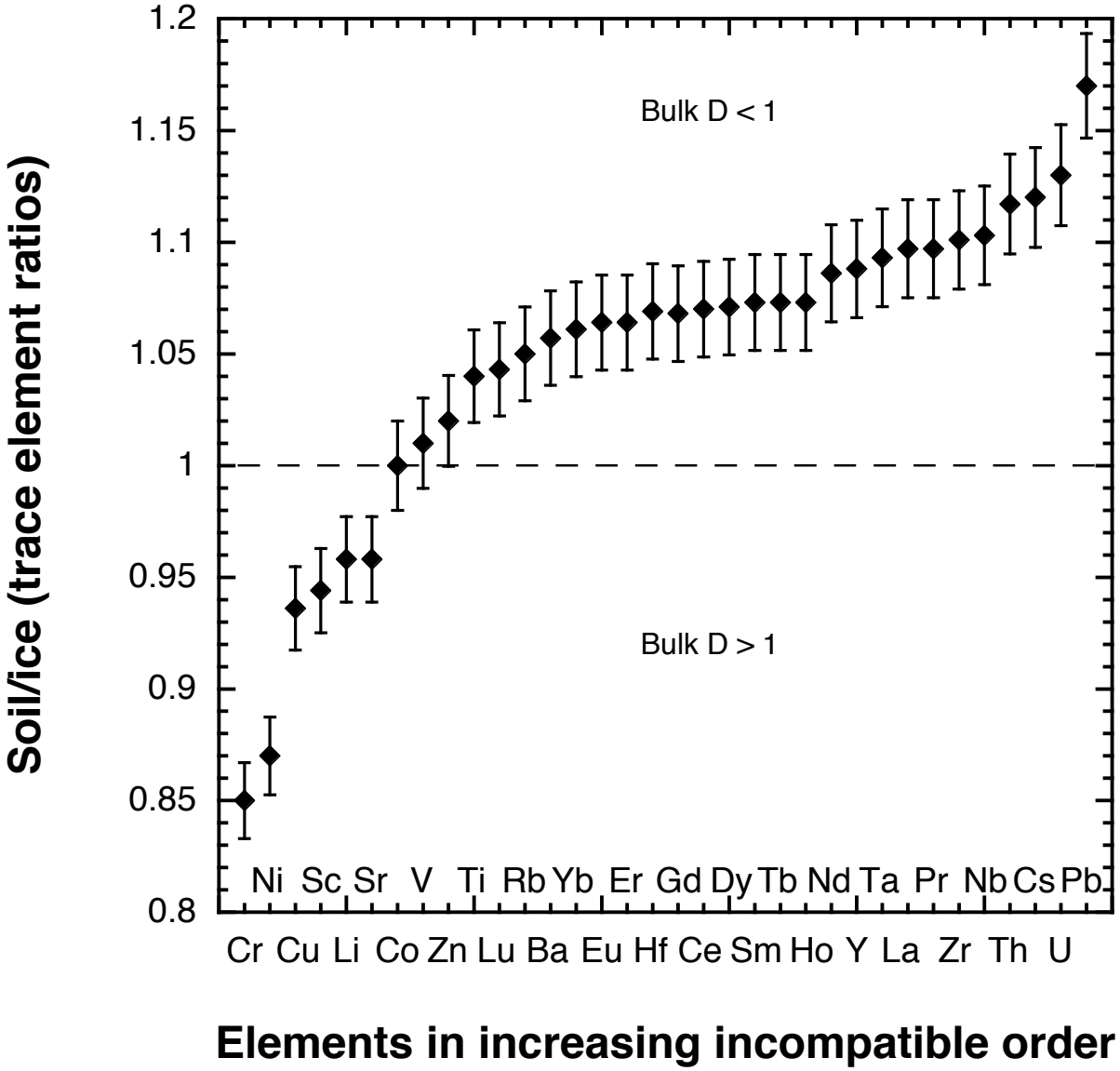

Figure

Click here to download Figure: Fig. 4.pdf

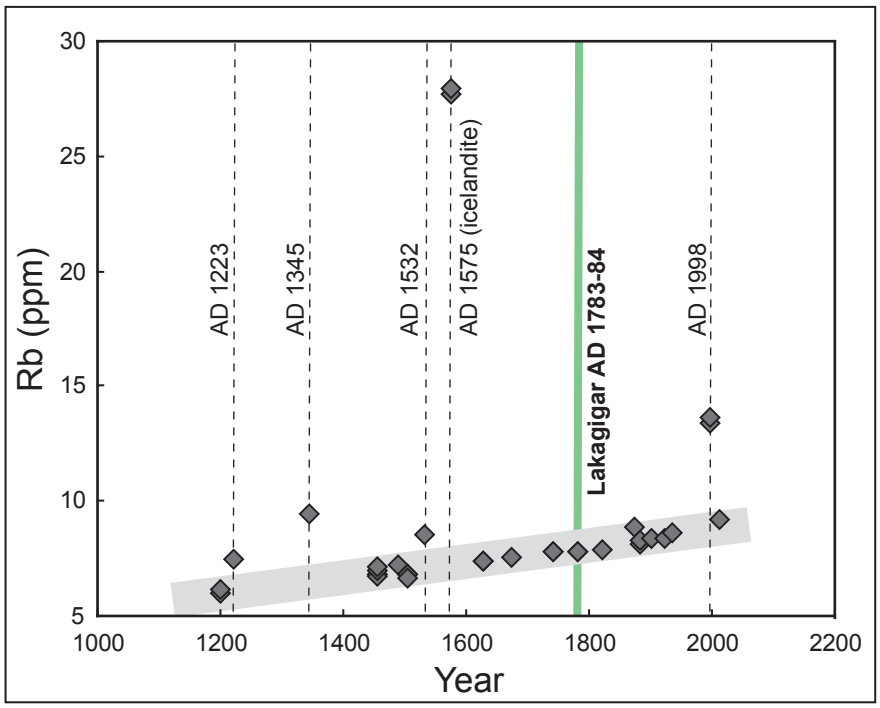

Figure

Click here to download Figure: Fig. 5.pdf

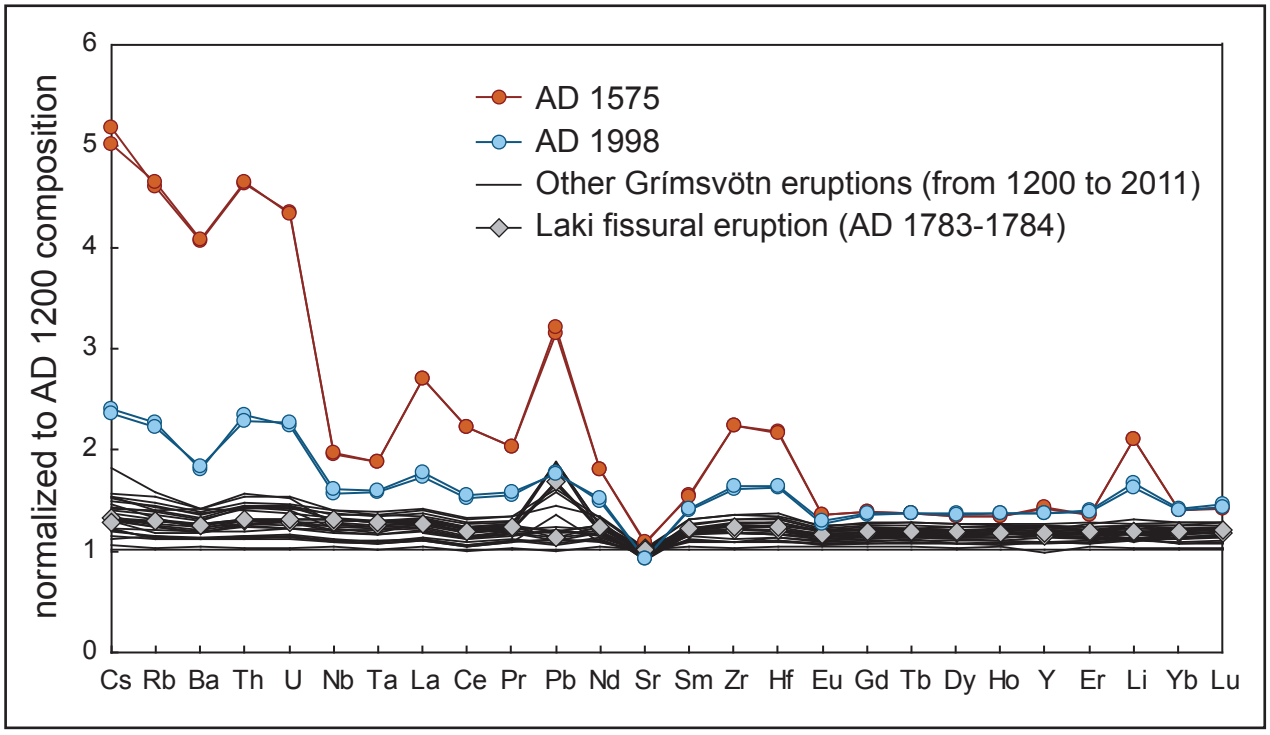

Figure

Click here to download Figure: Fig. 6.pdf

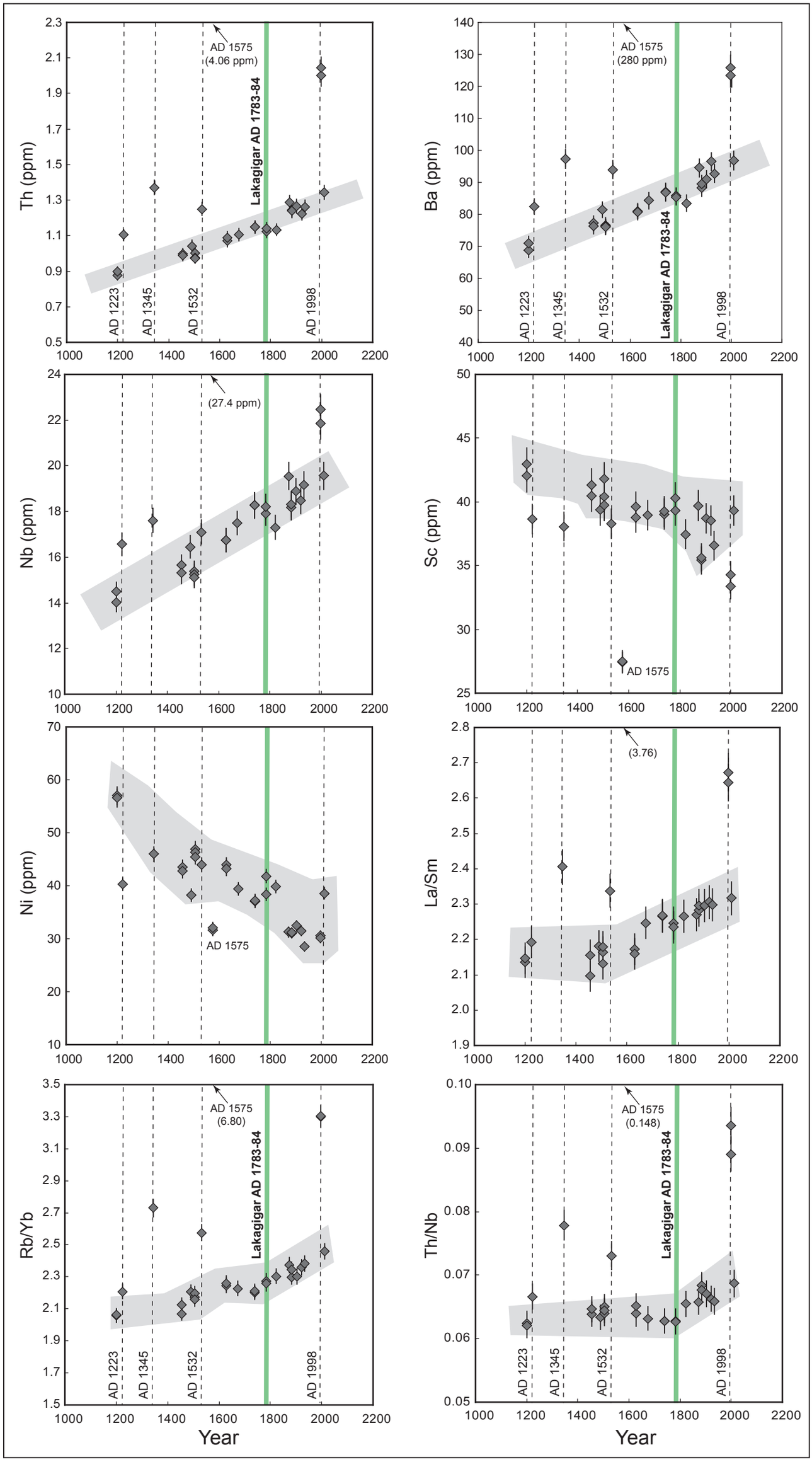

Figure

Click here to download Figure: Fig. 7.pdf

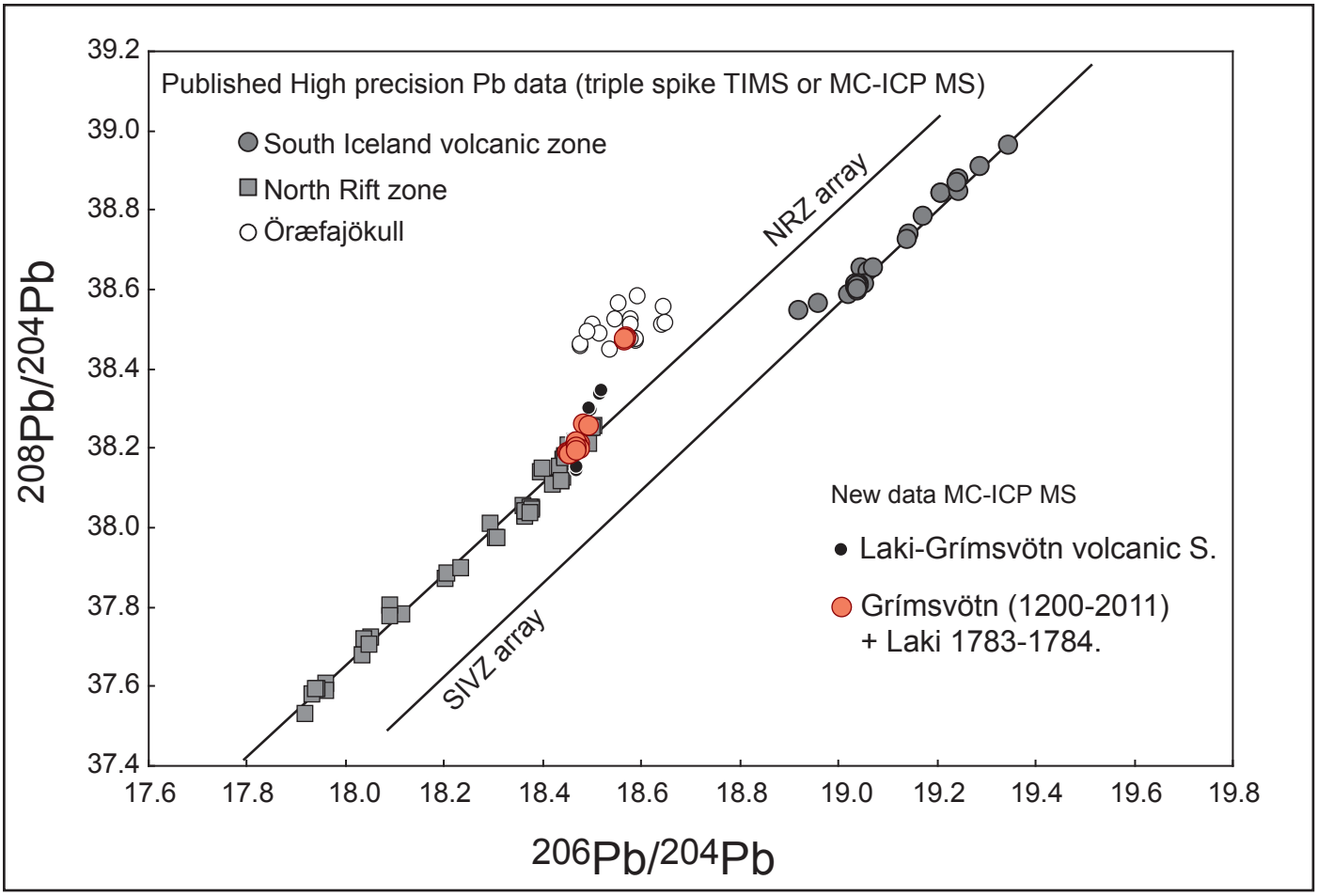

Figure

Click here to download Figure: Fig. 8.pdf

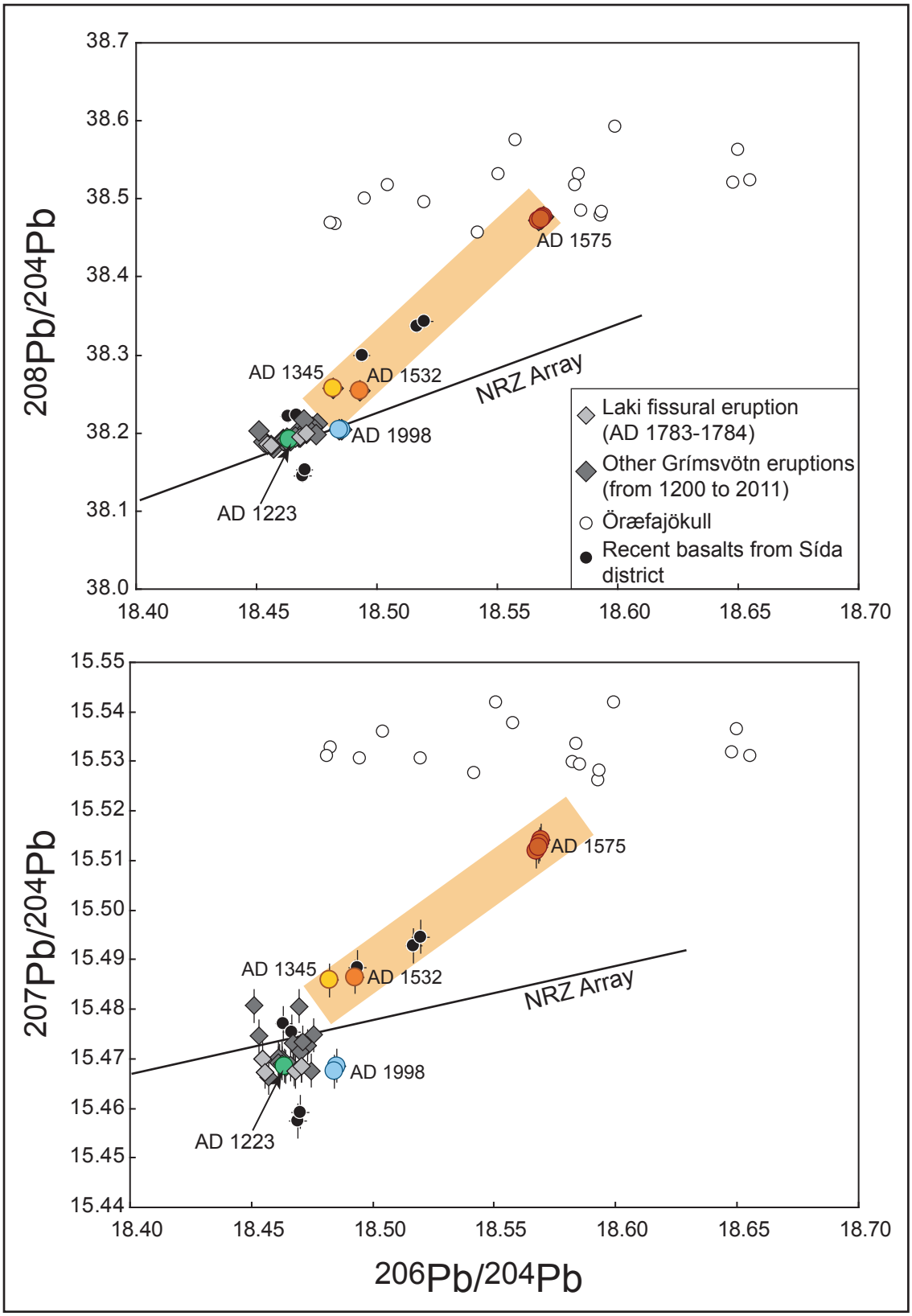

Figure

Click here to download Figure: Fig.9.pdf

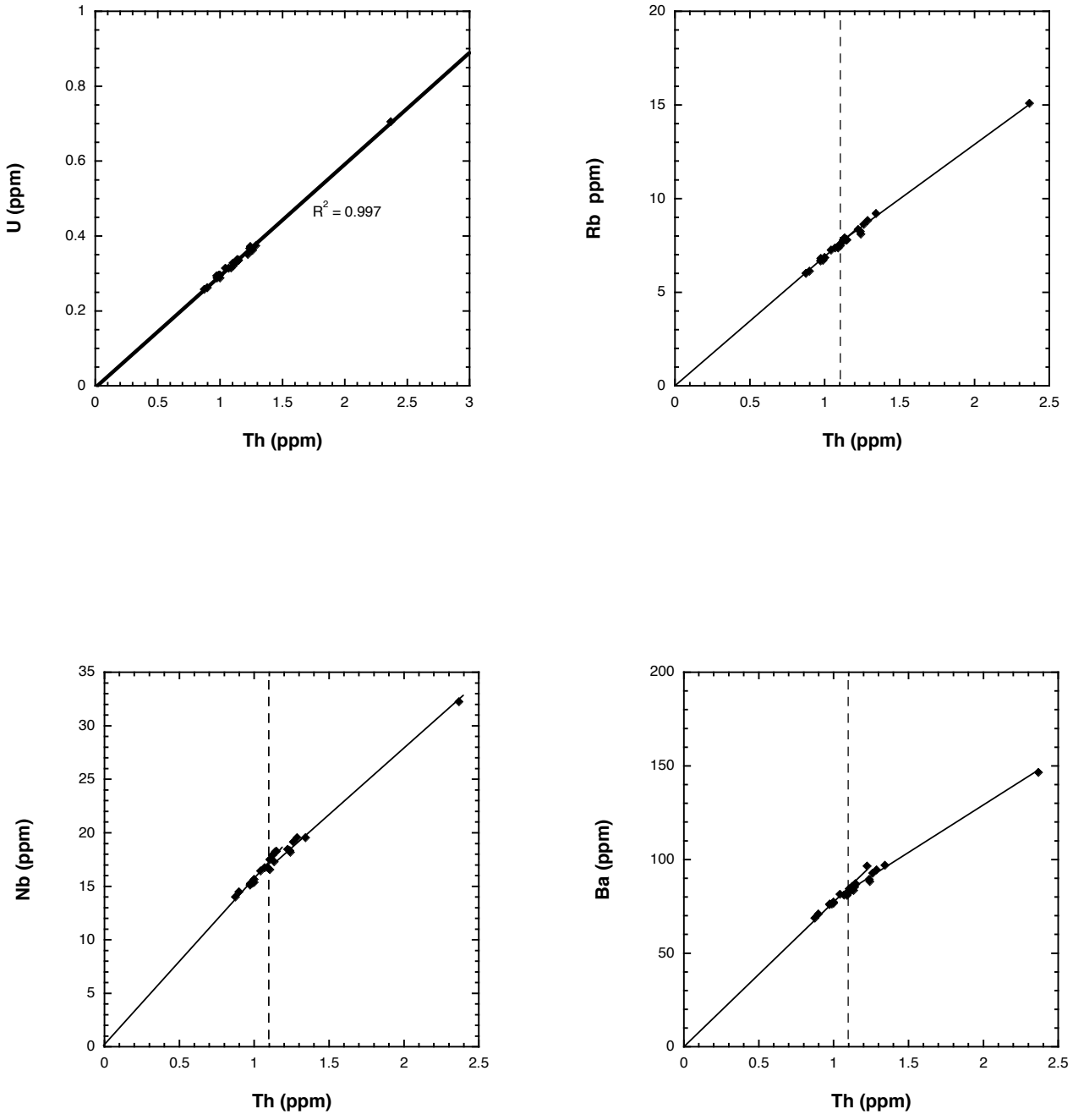

Figure

Click here to download Figure: Fig. 10.pdf

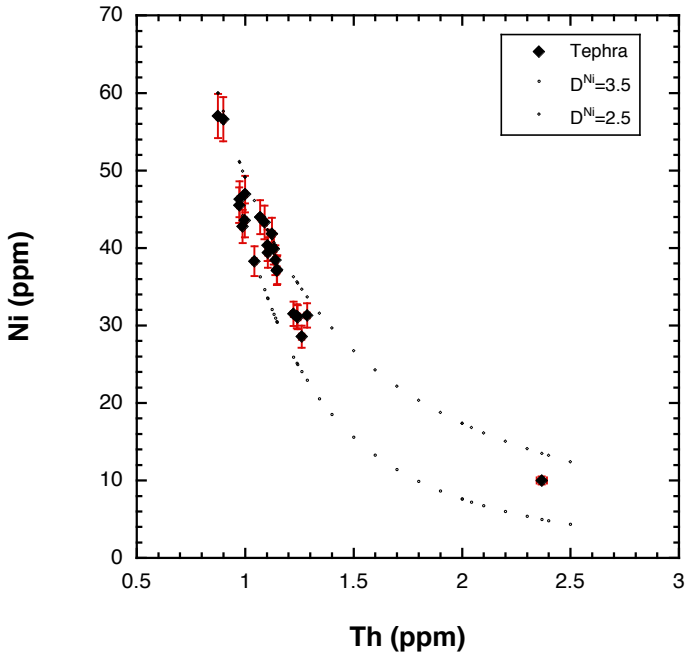

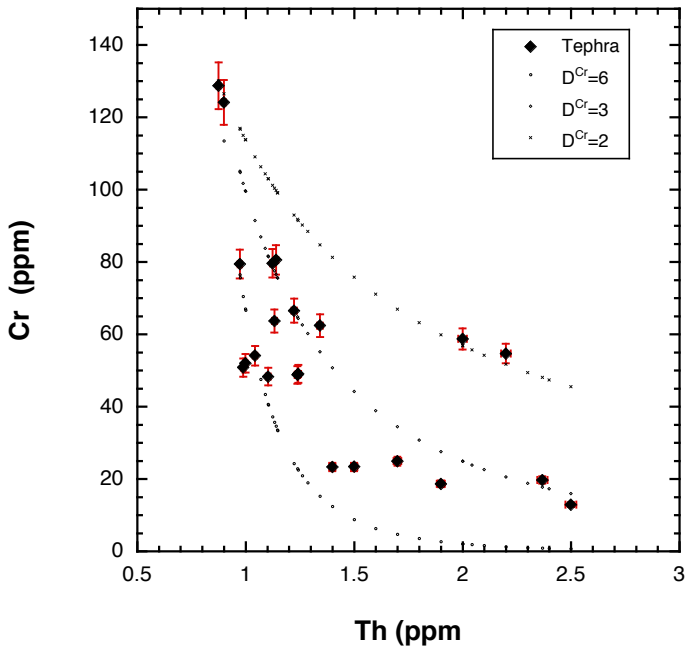

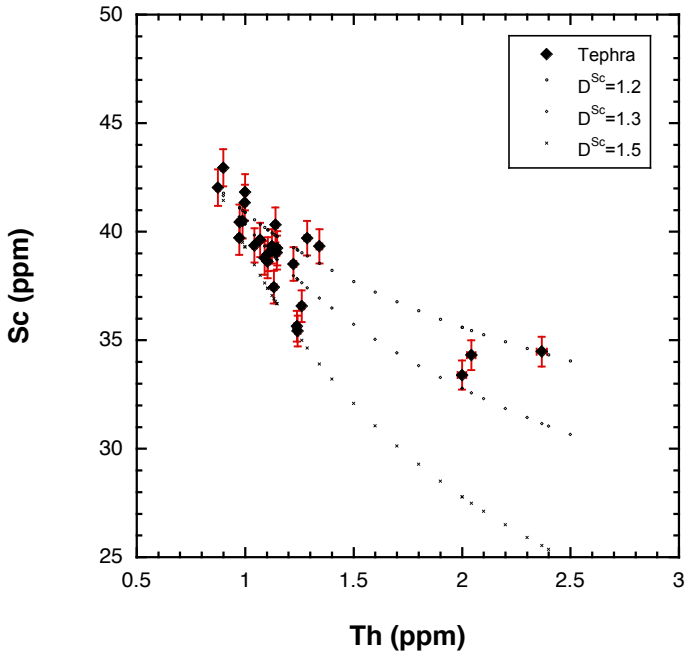

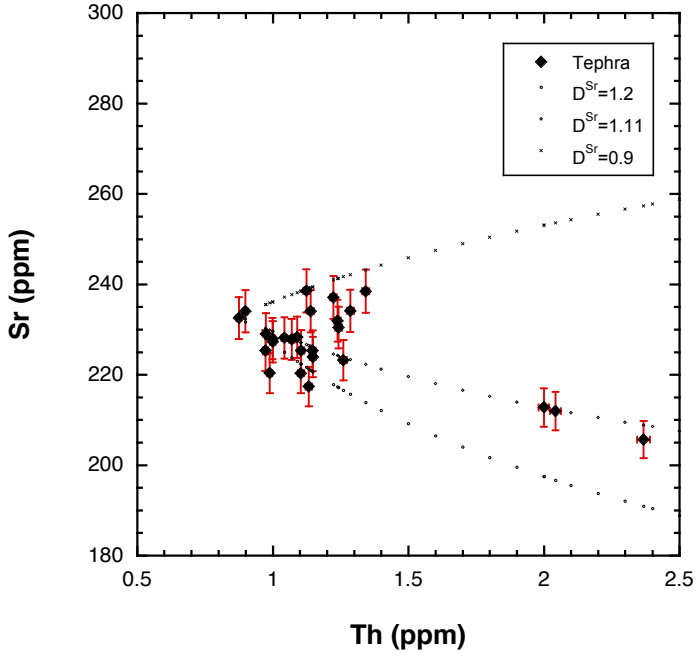

Figure
Click here to download Figure: Fig. 11.pdf

Figure 11

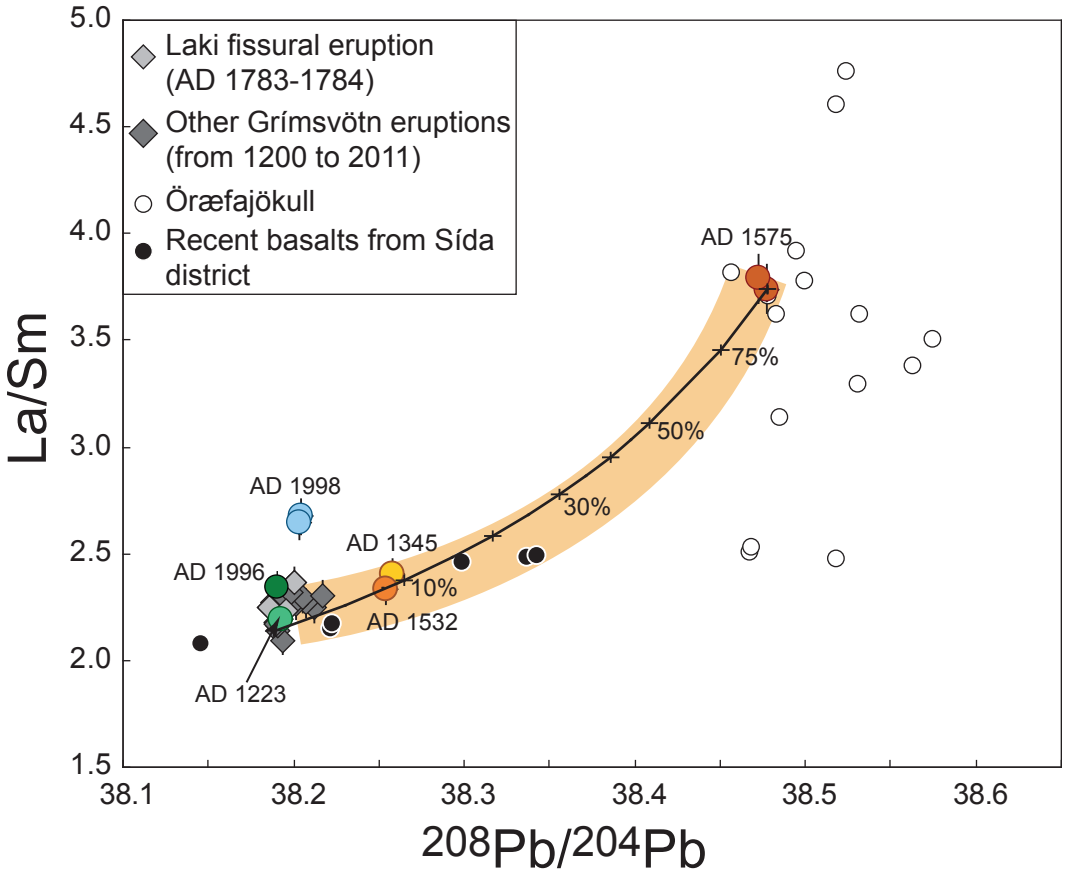

Table

Click here to download Table: Table 1_Sigmarsson.pdf

Table 1. Whole-rock trace element concentration in historical tephra from Grímsvötn volcano, Iceland

Sample	G-1200	G-1223	G-1345	G-1455A	G-1455B	G-1490	G-1505	G-1532	G-1575	G-1629	G-1674	G-1740
Li	6.01	6.97	7.46	6.71	6.50	6.92	6.58	7.19	12.6	6.75	7.02	7.27
Sc	42.0	38.6	38.1	41.3	38.2	39.4	41.8	38.3	27.4	39.6	39.0	39.0
Ti	14274	15419	13993	15188	15632	15402	15166	15022	10015	15279	15964	16455
V	363	381	354	381	377	377	375	363	212	374	387	394
Cr	129	48.3	59.0	52.0	43.2	54.1	79.4	69.7	59.9	79.6	63.7	49.0
Co	48.3	47.5	46.0	47.9	47.6	46.6	48.3	46.7	31.1	174	47.2	47.7
Ni	57.0	40.3	46.0	43.5	37.3	38.3	46.9	43.9	31.6	44.0	39.4	37.1
Cu	128	111	116	119	109	108	115	110	66.5	108	106	103
Zn	111	119	116	119	118	118	116	116	104	120	122	122
Rb	6.01	7.48	9.42	6.85	7.01	7.25	6.84	8.54	27.7	7.37	7.57	7.81
Sr	233	220	209	228	211	228	227	229	249	228	225	225
Y	32.0	37.0	37.7	35.8	37.6	36.5	34.7	36.8	45.0	36.6	38.0	39.3
Zr	148	174	181	166	177	174	161	179	331	174	178	184
Nb	14.0	16.6	17.6	15.6	16.9	16.4	15.4	17.1	27.3	16.7	17.5	18.3
Cs	0.062	0.084	0.114	0.074	0.080	0.076	0.069	0.095	0.324	0.081	0.081	0.085
Ba	68.7	82.5	97.3	77.3	80.6	81.4	76.7	94.0	279	81.1	84.3	87.0
La	11.0	13.2	14.4	12.3	13.4	13.1	12.2	14.0	29.8	12.9	13.6	14.2
Ce	28.8	32.0	34.6	31.0	32.6	32.6	30.4	34.2	64.1	32.1	33.8	35.1
Pr	4.02	4.71	4.90	4.45	4.82	4.70	4.41	4.83	8.13	4.61	4.84	4.99
Nd	18.7	22.1	22.4	21.0	22.5	22.0	20.4	22.3	33.7	21.5	22.6	23.4
Sm	5.15	6.02	5.98	5.89	6.10	6.00	5.64	5.99	7.96	5.94	6.07	6.27
Eu	1.81	2.05	1.96	1.97	2.08	2.07	1.94	2.06	2.46	2.00	2.09	2.17
Gd	6.10	7.03	7.00	6.73	7.16	6.95	6.59	6.98	8.39	6.91	7.13	7.34
Tb	0.958	1.10	1.11	1.08	1.13	1.10	1.06	1.09	1.31	1.08	1.13	1.16
Dy	6.00	6.89	6.96	6.66	7.03	6.78	6.39	6.75	8.04	6.73	6.98	7.24
Ho	1.19	1.38	1.40	1.31	1.41	1.34	1.29	1.34	1.60	1.35	1.40	1.44
Er	3.32	3.84	3.90	3.67	3.88	3.77	3.55	3.73	4.47	3.71	3.87	3.97
Yb	2.92	3.39	3.45	3.22	3.43	3.29	3.15	3.32	4.07	3.28	3.40	3.55
Lu	0.415	0.486	0.487	0.475	0.485	0.483	0.455	0.466	0.587	0.479	0.491	0.506
Hf	3.77	4.45	4.65	4.22	4.53	4.38	4.15	4.53	8.20	4.36	4.51	4.67
Ta	0.915	1.06	1.12	1.00	1.09	1.05	0.980	1.07	1.71	1.99	1.12	1.17
Pb	0.826	0.934	1.53	0.883	1.01	0.910	0.906	1.39	2.60	0.985	1.36	0.982
Th	0.875	1.10	1.37	0.999	1.10	1.04	1.00	1.25	4.05	1.07	1.11	1.15
U	0.258	0.328	0.390	0.296	0.333	0.314	0.288	0.361	1.12	0.314	0.320	0.335

Sample	L-4 Laki-lava	M-1 Laki-tephra	L-84 Laki-lava	G-1823	G-1873	G-1883	G-1903	G-1922	G-1934	G-1998	G-2011	Gjá-12 Gjálp 1996
Li	7.09	7.15	7.14	6.64	7.56	7.05	7.44	7.44	7.47	9.70	7.87	12.2
Sc	39.3	40.3	39.0	37.4	39.7	35.4	38.7	38.5	36.6	33.4	39.3	34.5
Ti	16127	16735	16268	15450	17801	15733	16541	16232	16735	16523	17232	14614
V	392	400	395	378	422	379	398	391	392	383	402	134
Cr	66.6	58.7	56.4	62.4	19.7	23.3	25.0	24.9	18.6	27.2	54.7	12.9
Co	47.6	47.8	47.7	45.0	47.6	44.7	46.2	45.2	44.9	43.0	47.7	31.5
Ni	41.8	38.4	39.2	39.8	31.3	31.0	32.4	31.5	28.5	30.6	38.6	10.0
Cu	106	98.8	88.6	111	121	103	101	111	105	85.2	102	37.7
Zn	125	126	129	126	132	120	124	163	125	125	133	171
Rb	7.79	7.79	7.95	7.90	8.83	8.11	8.37	8.35	8.62	13.4	9.20	15.1
Sr	239	234	232	217	234	230	228	237	223	213	238	206
Y	36.6	37.7	38.8	37.4	40.6	38.0	39.3	39.6	40.0	43.6	38.6	73.9
Zr	179	183	185	178	201	186	193	189	194	243	200	367
Nb	17.9	18.2	18.6	17.3	19.6	18.2	18.9	18.5	19.2	22.5	19.6	32.2
Cs	0.082	0.079	0.086	0.091	0.096	0.087	0.095	0.088	0.093	0.147	0.097	0.161
Ba	85.7	85.4	106	83.5	94.5	88.3	90.9	96.5	92.8	126	96.9	147
La	13.9	13.9	14.2	13.5	15.3	14.3	14.8	14.4	15.0	19.5	15.5	28.7
Ce	34.1	34.2	35.0	32.7	37.4	34.7	36.2	35.4	36.8	44.7	37.9	70.0
Pr	4.91	4.92	4.99	4.75	5.35	5.00	5.14	5.08	5.21	6.31	5.39	9.97
Nd	22.8	22.9	23.4	22.1	24.8	23.4	23.9	23.6	24.2	28.3	25.0	46.2
Sm	6.19	6.22	6.19	5.96	6.74	6.27	6.43	6.26	6.52	7.29	6.71	12.3
Eu	2.12	2.11	2.10	2.05	2.25	2.15	2.18	2.15	2.21	2.33	2.24	3.87
Gd	7.15	7.23	7.34	7.02	7.73	7.33	7.53	7.40	7.59	8.31	7.77	13.9
Tb	1.13	1.14	1.16	1.11	1.22	1.15	1.17	1.17	1.19	1.30	1.22	2.16
Dy	7.05	7.12	7.16	6.92	7.55	7.08	7.36	7.22	7.40	8.13	7.56	13.3
Ho	1.40	1.40	1.42	1.38	1.51	1.43	1.46	1.44	1.48	1.62	1.50	2.65
Er	3.90	3.92	3.98	3.87	4.22	3.97	4.10	3.99	4.10	4.58	4.21	7.40
Yb	3.42	3.45	3.50	3.43	3.72	3.53	3.63	3.54	3.62	4.05	3.74	6.61
Lu	0.489	0.496	0.498	0.488	0.528	0.503	0.531	0.510	0.518	0.591	0.529	0.973
Hf	4.53	4.63	4.70	4.54	5.02	4.81	4.89	4.78	4.95	6.15	5.15	8.66
Ta	1.14	1.16	1.20	1.12	1.24	1.19	1.23	1.19	1.22	1.45	1.27	2.07
Pb	1.39	0.934	4.45	0.960	1.33	1.55	2.67	8.54	1.31	1.44	1.19	1.78
Th	1.12	1.14	1.08	1.13	1.29	1.24	1.27	1.22	1.26	2.00	1.34	2.37
U	0.330	0.337	0.344	0.331	0.374	0.372	0.370	0.351	0.362	0.584	0.393	0.705

Table

Click here to download Table: Table 2_Sigmarsson.pdf

Table 2 Isotope ratios of historical Grímsvötn tephra

Sample	$^{87}Sr/^{86}Sr$	2 σ_m	$^{143}Nd/^{144}Nd$	2 σ_m	$^{206}Pb/^{204}Pb$	2 σ_m	$^{207}Pb/^{204}Pb$	2 σ_m	$^{208}Pb/^{204}Pb$	2 σ_m	MC-ICPMS
G-1200	0.703234	0.000011	0.513030	0.000006	18.4641	0.0011	15.4683	0.0012	38.1907	0.0034	Nu
G-1200 DR	0.703231	0.000009									
G-1223	0.703234	0.000009	0.513024	0.000005	18.4638	0.0012	15.4685	0.0011	38.1922	0.0030	Neptune
G-1345	0.703227	0.000007	0.513020	0.000005	18.4819	0.0015	15.4859	0.0013	38.2580	0.0036	Neptune
G-1455A	0.703227	0.000008	0.513030	0.000007	18.4627	0.0012	15.4701	0.0013	38.1934	0.0037	Nu
G-1455B	0.703242	0.000008	0.513020	0.000005	18.4519	0.0012	15.4738	0.0011	38.1901	0.0031	Neptune
G-1490	0.703223	0.000006	0.513020	0.000006	18.4618	0.0012	15.4696	0.0011	38.1900	0.0026	Neptune
G-1490 DD	0.703230	0.000010	0.513024	0.000007	18.4613	0.0011	15.4702	0.0009	38.1918	0.0023	Neptune
G-1505	0.703227	0.000007	0.513027	0.000006	18.4611	0.0012	15.4691	0.0012	38.1909	0.0031	Nu
G-1532	0.703251	0.000009	0.513014	0.000006	18.4928	0.0012	15.4864	0.0011	38.2538	0.0029	Neptune
G-1532 DR			0.513018	0.000005							
G-1575	0.703481	0.000009	0.512963	0.000005	18.5694	0.0009	15.5141	0.0008	38.4777	0.0021	Neptune
G-1575 DR					18.5687	0.0011	15.5133	0.0010	38.4751	0.0029	Neptune
G-1575 DD	0.703467	0.000007	0.512959	0.000006	18.5673	0.0010	15.5119	0.0009	38.4721	0.0024	Neptune
G-1575 DD DR					18.5681	0.0012	15.5128	0.0010	38.4747	0.0028	Neptune
G-1629	0.703241	0.000009	0.513022	0.000006	18.4625	0.0018	15.4691	0.0015	38.1897	0.0037	Nu
G-1674	0.703238	0.000007	0.513036	0.000005	18.4755	0.0022	15.4748	0.0019	38.2117	0.0049	Neptune
G-1674 DR	0.703242	0.000008									
G-1740	0.703240	0.000008	0.513028	0.000005	18.4674	0.0019	15.4679	0.0017	38.1949	0.0041	Neptune
G-1740 DD	0.703238	0.000007	0.513021	0.000006	18.4733	0.0013	15.4727	0.0012	38.2077	0.0035	Neptune
L-4	0.703238	0.000009	0.513028	0.000006	18.4545	0.0010	15.4700	0.0010	38.1856	0.0034	Nu
L-4 DD	0.703242	0.000008	0.513029	0.000006	18.4558	0.0017	15.4673	0.0016	38.1834	0.0033	Nu
M-1	0.703234	0.000006	0.513031	0.000007	18.4695	0.0011	15.4687	0.0011	38.1976	0.0030	Nu
L-84	0.703239	0.000007	0.513032	0.000005	18.4705	0.0012	15.4686	0.0011	38.2000	0.0032	Neptune
G-1823	0.703227	0.000011	0.513019	0.000005	18.4673	0.0016	15.4731	0.0015	38.2019	0.0037	Neptune
G-1873	0.703241	0.000007	0.513028	0.000006	18.4532	0.0016	15.4745	0.0016	38.1883	0.0042	Nu
G-1883	0.703224	0.000009	0.513028	0.000005	18.4701	0.0011	15.4715	0.0011	38.2019	0.0027	Neptune
G-1883 DD	0.703249	0.000009	0.513019	0.000006	18.4711	0.0013	15.4734	0.0012	38.2051	0.0031	Neptune
G-1903	0.703238	0.000013	0.513031	0.000005	18.4509	0.0011	15.4807	0.0010	38.2034	0.0026	Neptune
G-1922	0.703239	0.000009	0.513022	0.000006	18.4698	0.0011	15.4805	0.0010	38.2166	0.0028	Nu
G-1922 DD	0.703241	0.000007	0.513028	0.000006							
G-1934	0.703243	0.000012	0.513027	0.000005	18.4664	0.0013	15.4688	0.0011	38.1949	0.0027	Neptune
G-1998	0.703230	0.000008	0.513030	0.000005	18.4851	0.0012	15.4686	0.0011	38.2043	0.0028	Neptune
G-1998 DD	0.703229	0.000009	0.513030	0.000006	18.4844	0.0010	15.4674	0.0009	38.2036	0.0022	Neptune
G-2011	0.703233	0.000008	0.513025	0.000006	18.4746	0.0009	15.4676	0.0008	38.1980	0.0024	Nu
Gjá-12	0.703197	0.000008	0.513040	0.000006	18.4709	0.0008	15.4657	0.0008	38.1904	0.0026	Nu
Gjá-12 DR	0.703200	0.000007									
International reference materials:											
BCR-2 leached A	0.704996	0.000008	0.512630	0.000008							
BCR-2 leached B	0.704991	0.000007	0.512628	0.000006							
BCR-2 leached C					18.7947	0.0011	15.6217	0.0010	38.8173	0.0026	Nu
BCR-2 leached C DR					18.7979	0.0009	15.6243	0.0008	38.8236	0.0022	Neptune
BCR-2 unleached A					18.7464	0.0010	15.6239	0.0009	38.7190	0.0025	Neptune
BCR-2 unleached A DR					18.7465	0.0010	15.6229	0.0009	38.7166	0.0025	Neptune
BCR-2 unleached B					18.7524	0.0010	15.6226	0.0009	38.7245	0.0025	Neptune
BHVO-2 leached A	0.703464	0.000006	0.512979	0.000006							
BHVO-2 leached B	0.703466	0.000008	0.512976	0.000007	18.6344	0.0015	15.4919	0.0015	38.1949	0.0044	Nu
BHVO-2 leached C	0.703465	0.000009	0.512967	0.000006	18.6488	0.0013	15.4943	0.0012	38.2129	0.0032	Neptune
BHVO-2 unleached A					18.6715	0.0010	15.5408	0.0008	38.2535	0.0020	Neptune
BHVO-2 unleached B	0.703467	0.000007	0.512978	0.000007	18.6172	0.0011	15.5306	0.0009	38.2150	0.0024	Neptune
AGV-1 unleached A					18.9387	0.0010	15.6531	0.0009	38.5570	0.0022	Neptune
AGV-1 unleached A DR					18.9384	0.0010	15.6527	0.0009	38.5563	0.0024	Neptune
AGV-1 unleached B					18.9391	0.0008	15.6519	0.0007	38.5575	0.0018	Neptune
AGV-1 unleached B DR					18.9399	0.0010	15.6533	0.0009	38.5591	0.0026	Neptune
Comparison between Nu and Neptune Pb isotope ratio measurements:											
BCR-2 leached C					18.7947	0.0011	15.6217	0.0010	38.8173	0.0026	Nu
BCR-2 leached C DR					18.7979	0.0009	15.6243	0.0008	38.8236	0.0022	Neptune
Sample 1					19.1443	0.0010	15.5439	0.0009	38.7409	0.0029	Nu
Sample 1 DR					19.1429	0.0013	15.5424	0.0011	38.7356	0.0029	Neptune
Sample 2					19.2628	0.0014	15.5632	0.0012	38.9818	0.0045	Nu
Sample 2 DR					19.2631	0.0023	15.5631	0.0019	38.9843	0.0051	Neptune

Footnote: The abbreviations DD stands for duplicate dissolution and that of DR for duplicate runs; reported uncertainties are in-run errors. The isotope ratios of Sr and Nd are normalized to 87Sr/86Sr=0.710240 and 143Nd/144Nd=0.512100 for the NBS 987 and JNdi standards, respectively. Lead isotope ratios are given relative to NBS 981 values of 206Pb/204Pb=16.9405, 207Pb/204Pb=15.4963 and 208Pb/204Pb=36.7219 (Galer and Abouchami, 1998). Instrument used for Pb isotope ratios analyses is indicated. External reproducibility calculated using complete duplicate analyses of 7 samples among Grímsvötn-Laki suite is 0.000012 (17 ppm, 2σ) and 0.000005 (11 ppm) on the measured 87Sr/86Sr and 143Nd/144Nd ratios, respectively. For Pb isotopes, the 2σ external reproducibility is 0.0027 (145 ppm), 0.0026 (167 ppm) and 0.0059 (155 ppm) for 206Pb/204Pb, 207Pb/204Pb.

Table

Click here to download Table: Table 3_Sigmarsson.pdf

Table 3. Grímsvötn system since 1200 AD: Estimates of magma erupted and solidified in the crust and initial magma volume 800 years ago

	Magma temperature T_i (°C)	final rock temperature T_f (°C)	Energy release ΔE (KJ/kg)	Volume / century - min (km^3)	Volume / century - max (km^3)	Volume / 800 years (km^3)	Initial magma volume (km^3)
Geothermal:							
Case A	1200	200	1400	0.8	2.6	6 - 21	
Case B	1200	900	800	1.4	4.5	11 - 50	
Eruptions:							
Grímsvötn						8 - 12	
Laki 1783-84 (bulk lava density 2600 kg m^{-3}, magma density 2750 kg m^{-3})						14	
Total magma volume:							
Case A + eruptions, minimum						28	**80**
Case A + eruptions, maximum						47	**134**
Case B + eruptions, minimum						33	**94**
Case B + eruptions, maximum						76	**217**

Data on eruption sizes: Gudmundsson (2005), Jude-Eton et al., (2012), Hreinsdóttir et al. (2014), and Thordarson and Self (1993).

Data on energy release: Björnsson and Gudmundsson (1993).

Supplementary material for online publication only

Click here to download Supplementary material for online publication only: AppendiceTable 1.pdf